CATHODIC ELECTRODEPOSITION OF CADMIUM OXIDE, ZINC OXIDE AND MIXED CADMIUM OXIDE-ZINC OXIDE THIN FILMS

by

ASHWIN SESHADRI KALATHUR

Presented to the Faculty of the Graduate School of

The University of Texas at Arlington in Partial Fulfillment

of the Requirements

for the Degree of

MASTER OF SCIENCE IN MATERIALS SCIENCE AND ENGINEERING

THE UNIVERSITY OF TEXAS AT ARLINGTON

August 2005

ACKNOWLEDGEMENTS

With a deep sense of gratitude, I wish to express my sincere thanks to my supervisor, Prof. Krishnan Rajeshwar, for introducing me to the exciting field of semiconductor electrochemistry and for his extraordinary guidance and encouragement throughout this thesis project. I would also like to respectfully thank my committee members, Prof. Shashank Priya and Prof. J.-C. Chiao, for their helpful comments and advice.

My sincere thanks go to Drs. Norma Tacconi and C. R. Chenthamarakshan for the numerous discussions and remarkable help. I would also like to thank Ms. Shashikala Somasundaram and Mr. Yogeeswaran Ganesan for the helpful discussions. Finally, I would like to thank my parents and family for their constant support and encouragement.

July 25, 2005

ABSTRACT

CATHODIC ELECTRODEPOSITION OF CADMIUM OXIDE, ZINC OXIDE AND MIXED CADMIUM OXIDE-ZINC OXIDE THIN FILMS

Publication No. _____

Ashwin Seshadri Kalathur, M.S.

The University of Texas at Arlington, 2005

Supervising Professor: Krishnan Rajeshwar

Cadmium oxide (CdO) and $(CdO)_x(ZnO)_{1-x}$ mixed semiconductor films were cathodically electrodeposited for the first time on F-doped SnO_2 substrates. The CdO thin films were deposited from an aqueous 0.1 M KCl medium containing dissolved Cd^{2+} species and O_2. The $(CdO)_x(ZnO)_{1-x}$ mixed oxide films were deposited from a bath which contained Zn^{2+} in addition to the CdO bath constituents. Films were potentiostatically deposited at 80 ^{0}C followed by a post-deposition thermal anneal at 450 ^{0}C. The mechanism of the electrodeposition was explored using cyclic voltammetry. These samples were then analyzed by X-ray diffraction, scanning

electron microscopy, and UV-visible reflectance spectrophotometry. The photoelectrochemical behavior of these films is also presented. ZnO electrodeposition was carried out as a prelude to the main topic of this thesis research.

TABLE OF CONTENTS

LIST OF ILLUSTRATIONS

LIST OF TABLES

CHAPTER 1

INTRODUCTION AND BACKGROUND

1.1 Introduction

Transparent conducting oxides (TCOs) are materials that possess both high electrical conductivity and high optical transparency (> 80%) in the visible light region of the electromagnetic spectrum. These are remarkable materials in that the above properties are generally mutually exclusive and are hard to find in the same material. Cadmium oxide (CdO) is a n-type semiconductor with nearly metallic conductivity with a bandgap that varies from 2.2-2.4 eV. One of the ways of tailoring the band gap is by synthesis of new semiconductor phases with large/small band gap semiconductors. The band gap of cadmium oxide can be thus tuned over a wide range from 1.1 eV to 3.3 eV by alloying with suitable materials. These alloyed semiconductors have a number of interesting applications in electrochemical or photoelectrochemical devices, phototransistors, photodiodes, gas sensors, etc.

1.2 Electrochemical Deposition

An electrochemical deposition (electrodeposition) is achieved by passing an electric current between two or more electrodes separated by an electrolyte. The film deposition takes place at the electrode-electrolyte interface which is called the electrical

double layer. The basic electrochemical setup and a more detailed explanation of the system are given below.

The basic electrodeposition setup shown in Figure 1.1. consists of:

1. A working electrode (WE), which is the substrate on which the film is targeted to be formed.
2. A counterelectrode (CE), which can be an inert material like platinum or gold or in some cases a reactive material which helps in the synthesis of the film.
3. A reference electrode (RE), which measures the potential of the working electrode.
4. The electrodeposition bath, which is made up of a supporting electrolyte, additives, and the electroactive species.

An electrochemical cell is a heterogeneous system in which the reaction to produce the desired products takes place in a very small region at the interface of the working electrode and the bath known as the electrical double layer, which has a very high potential gradient of 10^5 V cm^{-1}. The product of the reaction is deposited as a thin film or coating on the working electrode. The solid-liquid interface present facilitates a conformal coating on the working electrode.

The two important parameters that determine the course of a reaction are

a. deposition current.
b. cell or working electrode potential.

Either of the two parameters mentioned can be controlled as a function of time. The control of the deposition current to form the product is known as galvanostatic

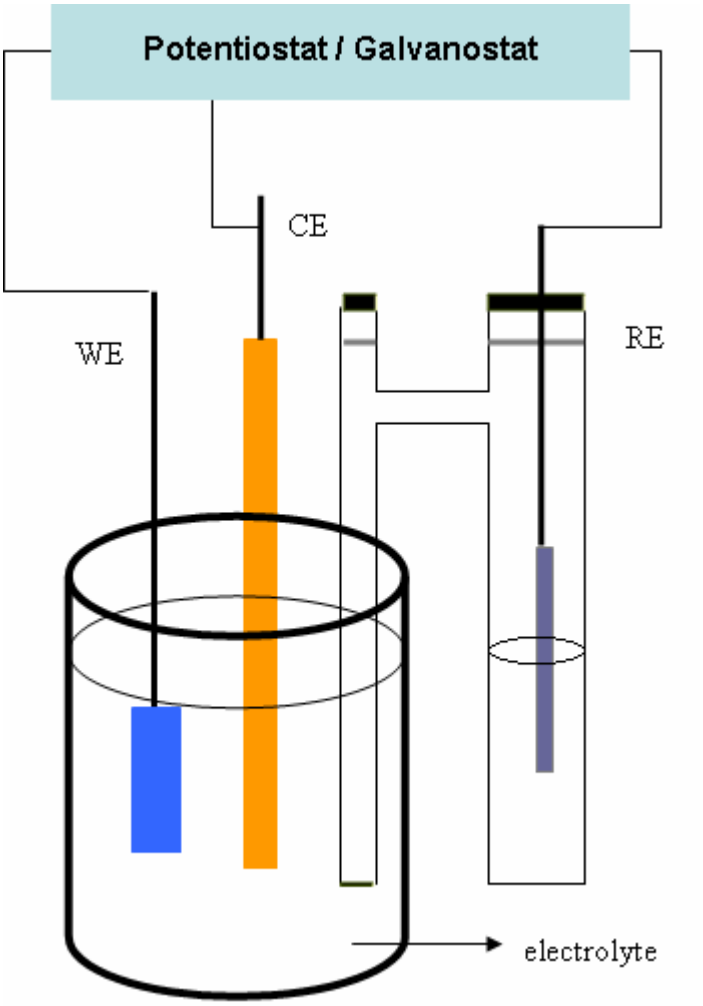

Figure 1.1 Schematic diagram of setup for electrodeposition of thin films. See text for definition of WE, CE and RE.

synthesis; the control of the cell potential to form the product is known as potentiostatic synthesis.

Galvanostatic synthesis: In galvanostatic synthesis, the current is controlled (frequently held constant), and the potential becomes the dependent variable, which is determined as a function of time. In this technique, a delicate control is exercised over the rate of the reaction which produces deposits with good adhesion and controlled morphology. However, the cell potential drifts as the reactant activity decreases. This drift in cell potential may lead to a multiplicity of products.

Potentiostatic synthesis: In potentiostatic synthesis the films are deposited by polarizing the working electrode to a desired potential with respect to a reference electrode. In this case, the cell current generally decays rapidly as the reaction proceeds, due to low rates of diffusion of the reactant molecules from the bulk to the electrode surface as well as due to decrease in activity of the reactant. However, the reaction is likely to yield a pure single phase product selected by the applied potential.

In general, advantages of electrochemical synthesis include the following:

1. It is a low temperature technique limited by the boiling point of the electrolyte. Molten salts (or ionic liquids) can be used if higher deposition conditions are required.

2. It is basically a reduction/oxidation reaction in which the fine tuning of the cell potential (or current in a galvanostatic mode) produces the desired products. This is something that is not easily achieved with chemical synthesis.
3. The film composition can be varied by varying the bath composition.
4. High quality products are possible at low cost.

On the other hand, disadvantages of electrochemical synthesis are:

1. It can be carried out only on conducting substrates.
2. As the process is carried out at relatively low temperatures the stoichiometry of the film is not as good as that obtained by high temperature processes.

1.3 Semiconductor Electrodeposition

Electrodeposition is an ancient art for depositing metals and metallic alloys such as copper, zinc, nickel and nickel based alloys, etc. The quality of these electrodeposited materials is excellent and coupled with the simplicity of the method and low costs have gone on to become industry standards. The most important of these is probably copper, which is used extensively in the semiconductor industry for back-end interconnects.

Electrochemical deposition involves the transfer of electrons across the interface which works very well for metals and metal alloys. However for semiconductors, the presence of a band gap can be a problem. In the case of cathodic deposition reactions, n-type semiconductors will be more likely deposited since electron transport is involved (unless light can be used for p-type), and the opposite for anodic deposition.

Semiconductor electrodeposition[1] is an exciting field which holds a lot of promise considering the low cost and generally low temperature and soft processing of materials. These attributes make it a much better route compared to the traditional vapor phase deposition of semiconductors from bulk material which is carried out at high temperature and is relatively very expensive. Figure 1.2 details the various inorganic semiconductors that have been electrodeposited, the dates, and the solvents used.

1.4 Metal Oxide Semiconductors

Metal oxide semiconductors such as titanium dioxide,[2-5] tungsten trioxide,[4-7] cuprous oxide[8-10] as well as a number of other oxides have been electrodeposited successfully. They have applications as transparent conducting oxides, materials for sensors, photocatalysts, high K-dielectrics, light emitting devices, etc. Many of the oxides are semiconductors with band gap values ranging from 1.0 eV to several eV.

Electrodeposition of Metal Oxides

The two popular methods of electrodeposition (Figures 1.3, 1.4) are based on:

a) Redox change (anodic)

In the electrochemical synthesis of metal oxides by redox change,[11] a metal ion or complex is oxidized at the electrode surface. The pH of solution is adjusted so that the initial oxidation state is stable, but the higher oxidation state readily undergoes

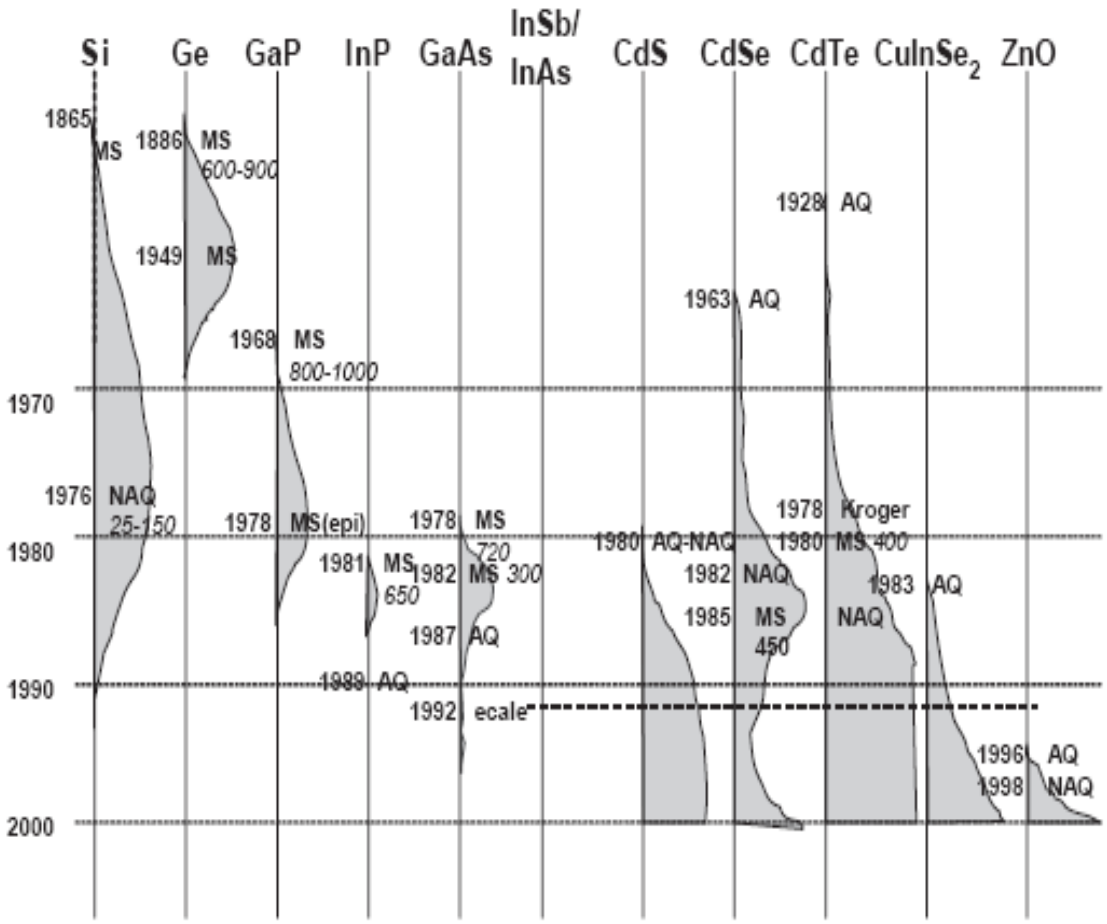

Figure 1.2 Electrodeposition of semiconductors over the years.[1]
Notations: AQ–aqueous, NAQ–non–aqueous, MS-molten salt. The figures to the right of the vertical bars represent the temperature of deposition and the ones to the left denote the year in which it was first carried out.

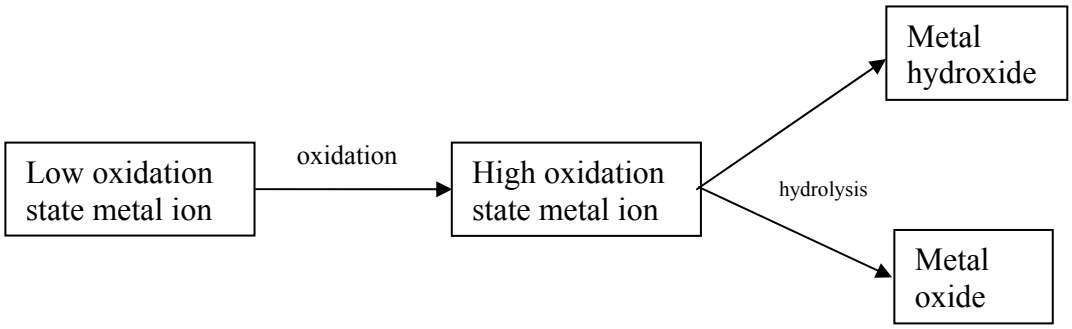

Figure 1.3 Electrodeposition of oxides by the redox change method.[11]

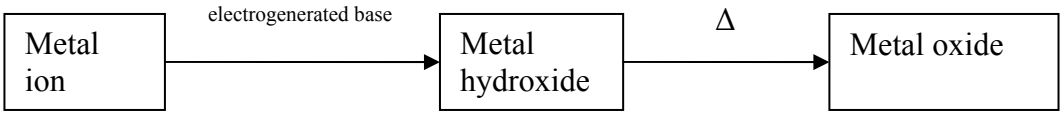

Figure 1.4 Electrodeposition of oxides by the electrogeneration of a base method.[11]

hydrolysis to form a metal hydroxide or an oxide. The flow diagram (Figure 1.3) lists the formation of metal oxides by this strategy.

b) Electrogeneration of base

In the electrogenerated base method,[11-13] the film is deposited on the cathode (which is the working electrode). Metal ions or complexes are then hydrolyzed by the electrogenerated base (Figure 1.4). The reactions are cathodic and include the reduction of water, sulfate, nitrate, etc. In the following sub-sections the structure and properties of cadmium oxide and zinc oxide which are ideal candidates for electrodeposition by this method will be briefly reviewed.

Cadmium Oxide

Cadmium oxide (CdO) is a n-type semiconductor with nearly metallic conductivity.[14-16] It has a direct energy band gap (E_g) of ~2.3 eV and two indirect transitions at lower energies.[17-19] The crystal structure of CdO is shown in Figure 1.5. The major optical transition at the higher energy and the value of E_g are both dependent on the defect concentration due to the Burstein-Moss effect.[20] The combination of high transparency in the visible range of the electromagnetic spectrum, high electrical conductivity, and high carrier concentration (even in non-doped samples because of inherent non-stoichiometry) of this material has prompted its use in CdO/CdTe heterostructure solar cells,[21] CdO/Cu_2O solar cells,[22] photoelectrochemical devices,[17,23-25] phototransistors,[26] photodiodes,[27] and gas sensors.[28] Solid solutions of CdO and ZnO have been investigated[29] for use as electrodes for the solar-assisted

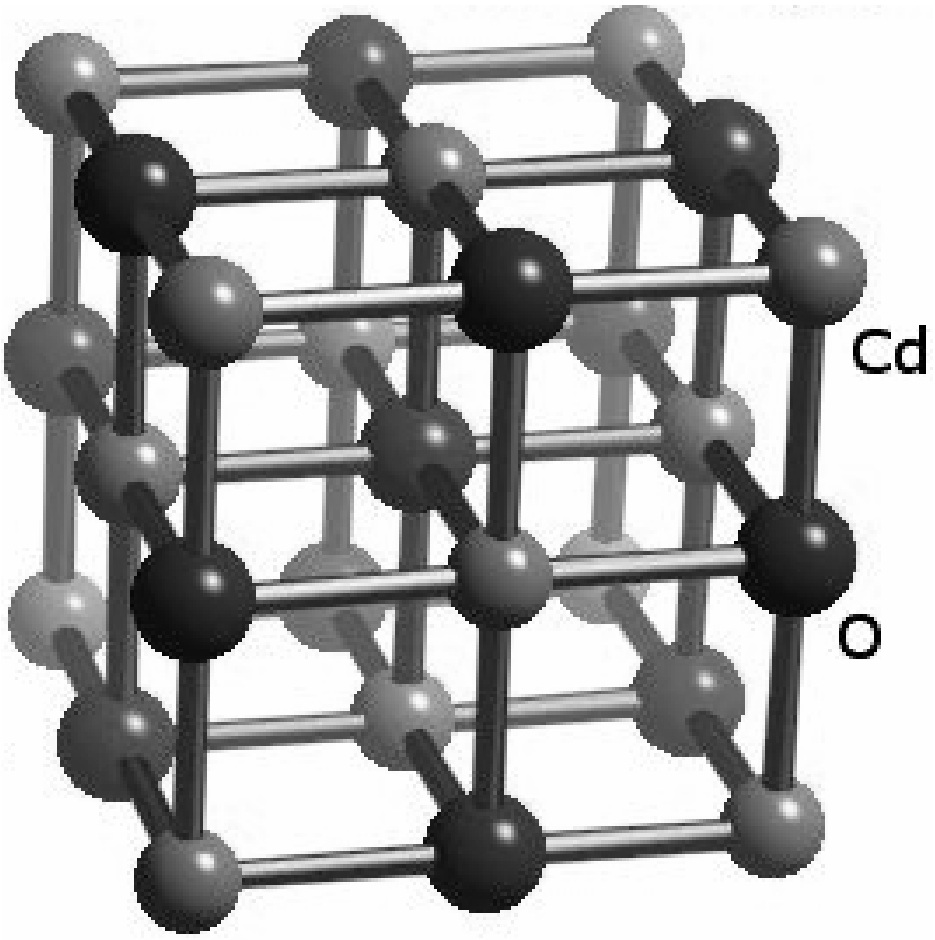

Figure 1.5 The crystal structure of CdO.

splitting of water and hydrogen generation. Thin films of CdO have been prepared by a variety of techniques including DC reactive magnetron sputtering,[30-32] activated reactive evaporation,[33,34] chemical bath deposition,[22,27] spray pyrolysis,[30,35-41] sol-gel process,[42-46] pulsed laser deposition,[20] ion beam sputtering,[21] Langmuir-Blodgett deposition,[47] and metal-organic chemical vapor deposition (MOCVD).[48,49]

To our knowledge, CdO has not been prepared in thin film form by cathodic electrodeposition from aqueous media. We are aware of only two prior reports[50,51] on the use of electrodeposition for preparing CdO thin films. In the first, metallic cadmium was first electrodeposited on Ti substrates (from an aqueous Cd^{2+}-ion containing medium) followed by thermal oxidation in air to convert Cd to CdO.[50] In a more recent study,[51] CdO films were electrodeposited on SnO_2-coated glass slides from a non-aqueous, dimethylsulfoxide bath containing dissolved oxygen gas and Cd^{2+} species.

Zinc Oxide

Zinc oxide is probably the most studied and versatile oxide semiconductor at present (other than TiO_2) with vast applications in varistors, sensors,[52,53] piezoelectric actuators,[54,55] lasers,[56] LEDs, etc. Zinc oxide is a wide band-gap n-type semiconductor with a band gap of 3.3– 3.5 eV. It has a direct band gap at room temperature, and an exciton binding energy of 60 meV. The combination of high excitonic energy and good high temperature characteristics makes ZnO a promising material for optical applications. Zinc oxide in the wurtzite form has a hexagonal structure (corresponding to space group *C*6*mc*) with lattice parameters $a = 0.3296$ and $c = 0.52065$ nm.

Table 1.1 lists the important properties of ZnO and Figure 1.6 shows tetrahedrally coordinated O^{2-} and Zn^{2+}ions stacked alternately along the *c*-axis.

Thin films of ZnO have been fabricated using a number of techniques such as sputtering,[54,57-64] sol-gel,[56,65-68] chemical vapor deposition,[69-73] spray pyrolysis,[74-78] molecular beam epitaxy,[79-81] as well as electrodeposition.[82-92] The fabrication via electrodeposition was first done in 1996[82,83] and since then it has been shown that high quality films on different substrates are possible. It has also been shown[84] that epitaxial films of ZnO can be grown on GaN substrate using electrodeposition. A number of bath formulations containing zinc chloride,[85,86] zinc nitrate,[87-90] hydrogen peroxide,[91] and zinc perchlorate[92] baths have been described for producing these films.

1.5 Outline of the Thesis

In this thesis work, thin films of CdO were synthesized for the first time by cathodic electrodeposition from an aqueous media. The deposition mechanism was investigated by cyclic voltammetry and studies were conducted to determine the crystal structure, transmittance, band gap, morphology, and composition of the films.

Thin films of mixed oxide, $(CdO)_x(ZnO)_{1-x}$ were deposited in an attempt to tune the band gap by varying the concentration of zinc and cadmium species in solution. These films show promising results which need to be further investigated. As a prelude to this work, ZnO films were successfully deposited on F-doped tin oxide with a preferred orientation along the c-axis.

Table 1.1 Important properties of ZnO.

Properties	**Value**	**Comment**
Band gap (at RT)	3.3 – 3.5 eV	Large band gap
Piezoelectric constant (e_{33})	1.2 Cm^{-2}	Largest among all semiconductors
Thermal conductivity	0.54 $Wcm^{-1}K^{-1.}$	Compared to 0.5 for GaAS
Exciton binding energy	60 meV	Largest of all II-VI and III –V compounds
Shear modulus	45.5 GPa	Shows high crystal stability
Lattice constants	a = 0.3296 c = 0.52065 nm	Wurtzite structure
Density	5600 kg m^{-3}	-

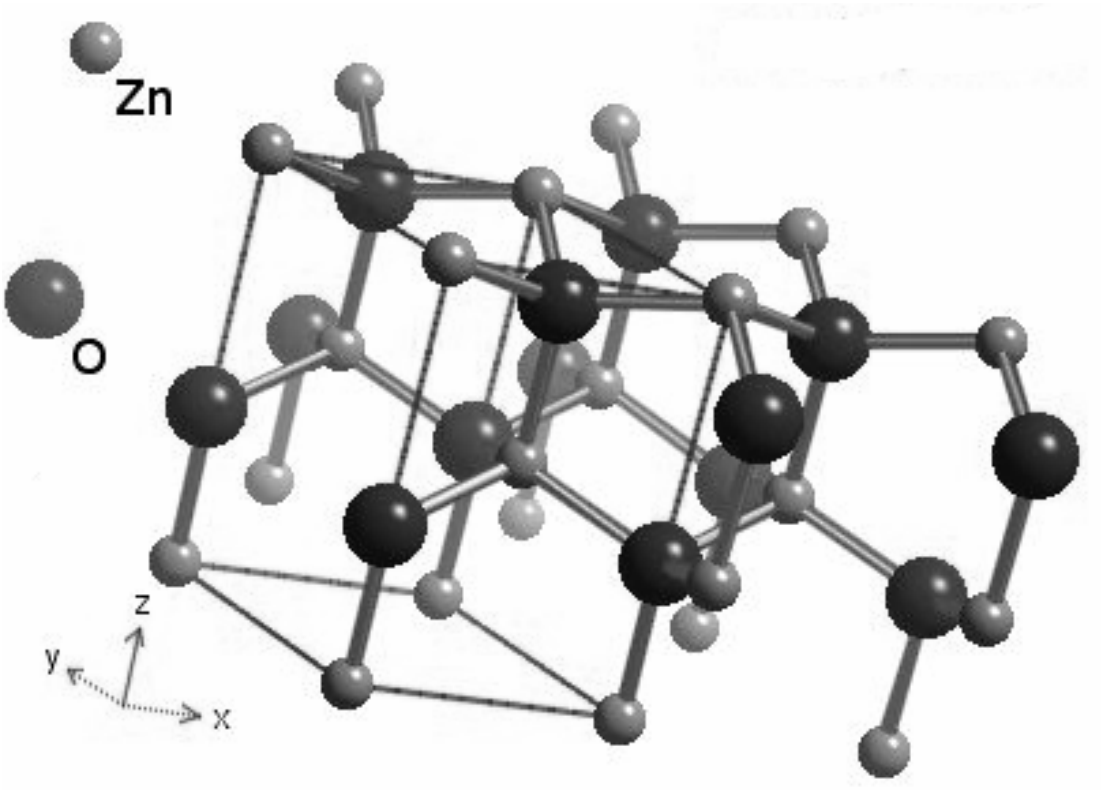

Figure 1.6 The crystal structure of ZnO.

CHAPTER 2

EXPERIMENTAL

All chemicals were from commercial sources and were the highest purity available. They were used without further purification. The transparent conducting oxide (TCO) substrates consisted of F-doped tin oxide (Nippon Sheet Glass Ltd.) coated on soda-lime glass. They were nominally ca. 400 nm thick and had a sheet resistance of 10.3 Ω. Strips (0.65 cm x 2 cm) were cut and cleaned in four 5 min steps of cleansing in ultrasonicated acetone, ethanol, 1:1 H_2O_2/ammonia, and finally ultrapure water. All solutions in this study were prepared from double-distilled (Corning Megapure) water.

Cadmium oxide films were cathodically electrodeposited from a cadmium chloride deposition bath which consisted of 2.5 mM $CdCl_2$ and 0.1 M KCl. Films were grown at –0.75 V (*vs*. Ag|AgCl|satd. KCl reference; all potentials in this work are quoted with respect to this reference) for a nominal duration of 15 min. The deposition bath temperature was maintained at 80 ^{0}C. They were then subjected to a post-deposition thermal anneal at 450 ^{o}C for 1 h in air using a Model 650-14 Isotemp Programmable Muffle Furnace (Fisher Scientific). A linear heat ramp (at 10 ^{0}C/min) from room temperature to a pre-selected final temperature of 450 ^{0}C was followed by a 1 h equilibration at the final temperature. The samples were then allowed to cool via natural convection on the furnace back to the ambient condition.

Zinc oxide films were cathodically electrodeposited from a zinc chloride deposition bath which consisted of 5 mM $ZnCl_2$ and 0.1 M KCl. Films were grown at –0.95 V and the deposition bath temperature was varied from 50 ^{0}C–90 ^{0}C. They were then subjected to a post-deposition thermal anneal at 500 ^{0}C for 1 h in a furnace operating at similar conditions as for the cadmium chloride anneal.

Mixed oxide films, $(ZnO)_x(CdO)_{1-x}$, were cathodically electrodeposited from an electrodeposition bath which contained different ratios of zinc chloride and cadmium chloride in solution (Table 2.1). The supporting electrolyte was 0.1 M KCl. The films were grown at –0.95 V. The deposition bath temperature was maintained at 80 ^{0}C. They were then subjected to a post-deposition thermal anneal at 450 ^{0}C for 1 h in a furnace operating at similar conditions as for the cadmium chloride anneal.

Table 2.1 Ratio of Zn^{2+}: Cd^{2+} species in solution for electrodepositing $(ZnO)_x(CdO)_{1-x.}$ films.

	Zinc chloride	**Cadmium chloride**
ZnO	5 mM	-
90 : 10	4.5 mM	0.5 mM
70 : 30	3.5 mM	1.5 mM
50 : 50	2.5 mM	2.5 mM
CdO	-	5 mM

A standard single-compartment, three-electrode electrochemical cell was used both for film preparation and for the photocurrent measurements. A Pt coil and a Ag|AgCl| satd. KCl reference electrode (Microelectrode Inc.), along with the TCO substrate as the working electrode, completed the cell set-up. All electrodeposition baths were sparged with ultrapure O_2 for 30 min prior to use and an O_2 overpressure was maintained during film deposition. Selected depositions (aimed at forming a metallic cadmium layer on the substrate) also used a de-oxygenated bath obtained by purging pre-purified N_2 through it and preventing re-oxygenation with a N_2 blanket. Depositions were carried out at 80 ^{0}C and measurements were performed at the laboratory ambient temperature (25 ± 2 ^{o}C).

Electrodeposition was carried out on a 100A Electrochemical Analyzer [Bioanalytical Systems (BAS), W. Lafayette, IN]. X-ray photoelectron spectroscopy (XPS) used a Perkin Elmer/Physical Electronics Model 5000C system with other details given elsewhere. Photovoltammetry was performed on a Model CV-27 BAS Voltammograph equipped with a Soltec X-Y recorder Model VP-6414S. The UV light source was a 75 W xenon arc lamp (Oriel, Stratford, CT) which had an output of 2.2 mW/cm^2 and the visible light source was a 100 W tungsten-halogen which had an output of ~0.95 mW/cm^{2}as measured with an Oriel Model 70260 Radiant Power/Energy meter. Films were cast on glass slides (25 mm x 25 mm) for diffuse reflectance spectroscopy. For scanning electron microscopy (SEM), a JEOL 845 instrument was used with a nominal electron beam voltage of 10 kV. Diffuse reflectance spectroscopy was done on a Perkin-Elmer Lambda 6 spectrophotometer. X-ray diffraction (XRD)

patterns of the samples were obtained on a Siemens D – 500 powder diffractometer using Cu Kα radiation. Auger electron spectra were acquired on a custom-built instrument fitted with a cylindrical mirror analyzer. An electron beam voltage of 3 kV and a beam current of 1 mA were used for sample excitation. The oxide sample surface was cleaned with an argon sputter gun prior to analyses.

CHAPTER 3

RESULTS AND DISCUSSION

3.1 Cadmium Oxide

The first study on the "electrogeneration of base" strategy[11-13] for preparing CdO thin films by cathodic electrodeposition from aqueous media is presented below. The mechanistic aspects of the film deposition process are briefly explored along with characterization of the deposited material by X-ray diffraction, scanning electron microscopy, and surface analysis techniques. Finally, the photoelectrochemical behavior of the deposited material is presented.

Cyclic voltammetry is carried out by applying a potential to the "working" electrode from an initial value, E_i, to a predetermined limit, E_f (known as the switching potential) where the direction is reversed. The current response is plotted as a function of the applied potential. Figure 3.1 contains cyclic voltammograms for the TCO working electrode in 0.1 M KCl supporting electrolyte. Three different solution conditions are considered and in each case, the scan was begun at 0 V in the negative direction upto the switch limit of -1.0 V and back to 0 V.

a) Scan with N_2 purge / O_2 purge (in the absence of Cd^{2+})

The control scan with N_2 purge through the supporting electrolyte and without Cd^{2+} species present was flat with near zero current and featureless and is not shown.

The forward scan with only dissolved O_2 present (no Cd^{2+} species) shows a reduction wave with onset around -400 mV and is assigned to the process:

$$\tfrac{1}{2}\, O_2 + H_2O + 2\, e^- \rightarrow 2\, OH^- \qquad [3.1]$$

The return scan tracks the forward one underlining the irreversibility of the above process and the continuing electrogeneration of the base.

b) Scan with Cd^{2+} ions in solution (absence of dissolved O_2)

In contrast to the above case, the forward scan with only Cd^{2+} species present in the electrolyte (no dissolved O_2) shows no evidence for the wave assigned to Reaction 3.1 (as expected) but instead shows a new reduction process with onset at ~ -760 mV. This wave is assigned to:

$$Cd^{2+} + 2\, e^- \rightarrow Cd \qquad [3.2]$$

The return scan does not track the forward one signaling a film deposition process along with the characteristic scan cross-over typically seen for a nucleation/growth process. An anodic curve follows with a peak at ~ -600 mV which is assigned to the stripping of Cd from the substrate surface:

$$Cd \rightarrow Cd^{2+} + 2\, e^- \qquad [3.3]$$

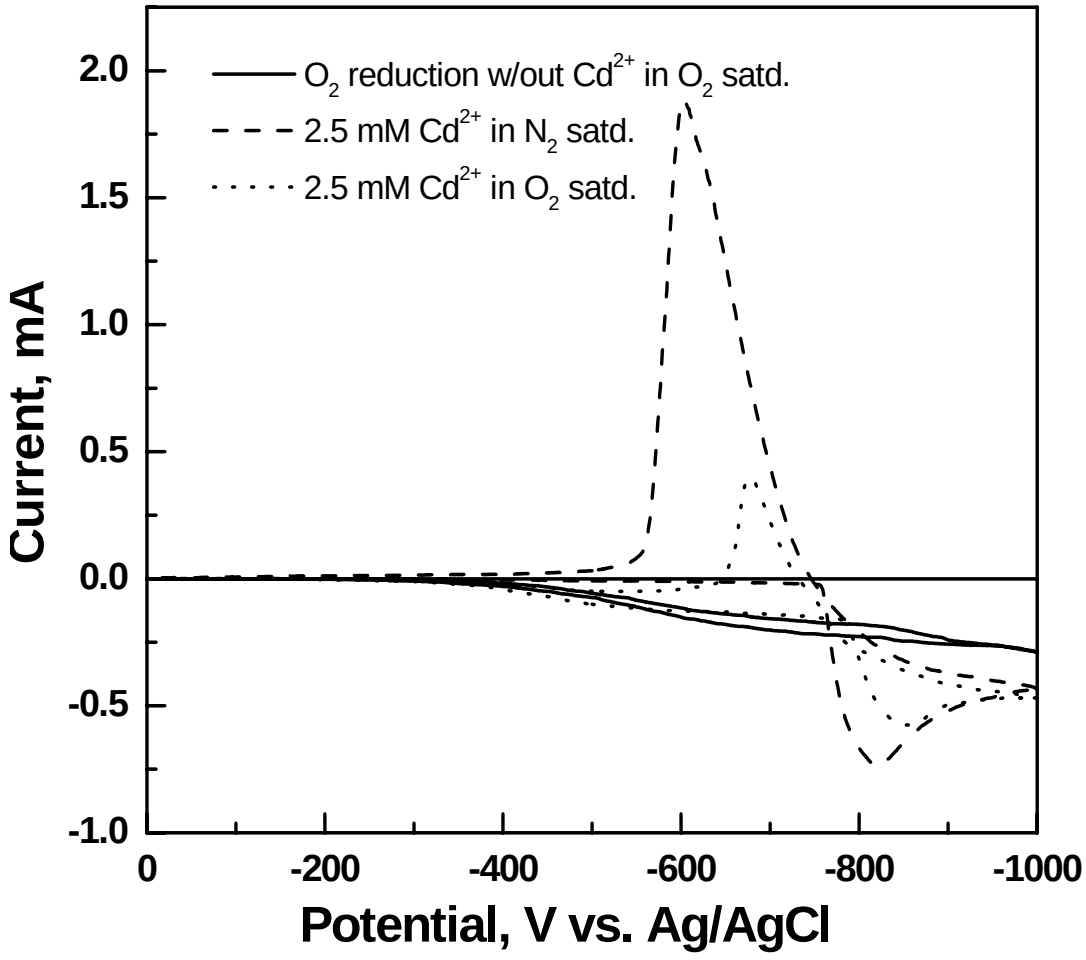

Figure 3.1 Cyclic voltammograms for a TCO electrode in three solutions as shown. The supporting electrolyte was 0.1 M KCl.

c) Scan with both Cd^{2+} and O_2 in solution

The third cyclic voltammogram in Figure 3.1 is most relevant in terms of this study and pertains to the case when both Cd^{2+} species and dissolved O_2 are present in the supporting electrolyte. The forward scan contains features common to both the cases considered above, but most importantly, the free Cd deposition wave is suppressed and shifted to more negative potentials around ~ -800 mV. The return scan shows a more marked cross-over than in the second cyclic voltammogram, and the anodic stripping wave is also drastically reduced with the peak shifting to ~ -680 mV. These trends can be accommodated by the three new processes:

$$Cd^{2+} + 2\,OH^- \rightarrow CdO + H_2O \qquad [3.4]$$

$$Cd^{2+} + \tfrac{1}{2}\,O_2 + 2e^- \rightarrow CdO \qquad [3.5]$$

$$Cd^{2+} + 2\,OH^- \rightarrow Cd(OH)_2 \qquad [3.6]$$

all contributing to film formation on the substrate surface. Note that Eqn. 3.5 can be regarded as a composite of Eqns. 3.1 and 3.4 respectively.

The extent of Eqns. 3.4-3.6 is controlled by variables such as negative switch limit of the scan, the potential scan rate, the amount of dissolved O_2 in the electrolyte, the Cd^{2+} ion concentration and the nature of the substrate. A detailed study of these variables is planned in the near future.

For ex situ analyses of the deposited material, films were potentiostatically deposited at selected potentials (that were guided by the cyclic voltammetry data) for

nominally 15 min. As mentioned earlier, these film depositions were done at 80 ^{0}C (instead of at ambient temperature) to obtain better-quality (more crystalline) films. For example, ZnO films are electrodeposited at temperatures well above ambient (see refs. 83, 84). After deposition, the thermal anneal in air serves to convert $Cd(OH)_2$ (see Eq. 3.7) to CdO:

$$Cd(OH)_2 \xrightarrow{\Delta} CdO + H_2O \qquad [3.7]$$

and also to convert any metallic Cd to CdO via the thermal counterpart of Eqn. 3.5. As is common to other oxide films, the post-deposition anneal also serves to complete the film crystallization process.

Figure 3.2 contains a representative XRD pattern for an electrodeposited CdO film treated as above. The (111), (200), and (220) reflections are clearly seen and closely match the reference patterns for CdO.[93] Additionally, a peak assignable to the SnO_2 substrate is also seen (Figure 3.2). The lattice constant for cubic crystals can be calculated using the expression:

$$a = d * \sqrt{h^2 + k^2 + l^2} \qquad [3.8]$$

The lattice constant value of 4.69 Å (at large θ values for more accuracy) calculated from the observed d-spacings are in excellent agreement with that reported (4.69 Å) for cubic CdO.[93] Table 3.1 lists the observed and expected d–spacing values for CdO.

Table 3.1 Observed and expected d-spacing for an electrodeposited CdO film.

	d (observed), Å	**d (JCPD), Å**
(111)	2.70	2.71
(200)	2.34	2.34
(220)	1.65	1.66

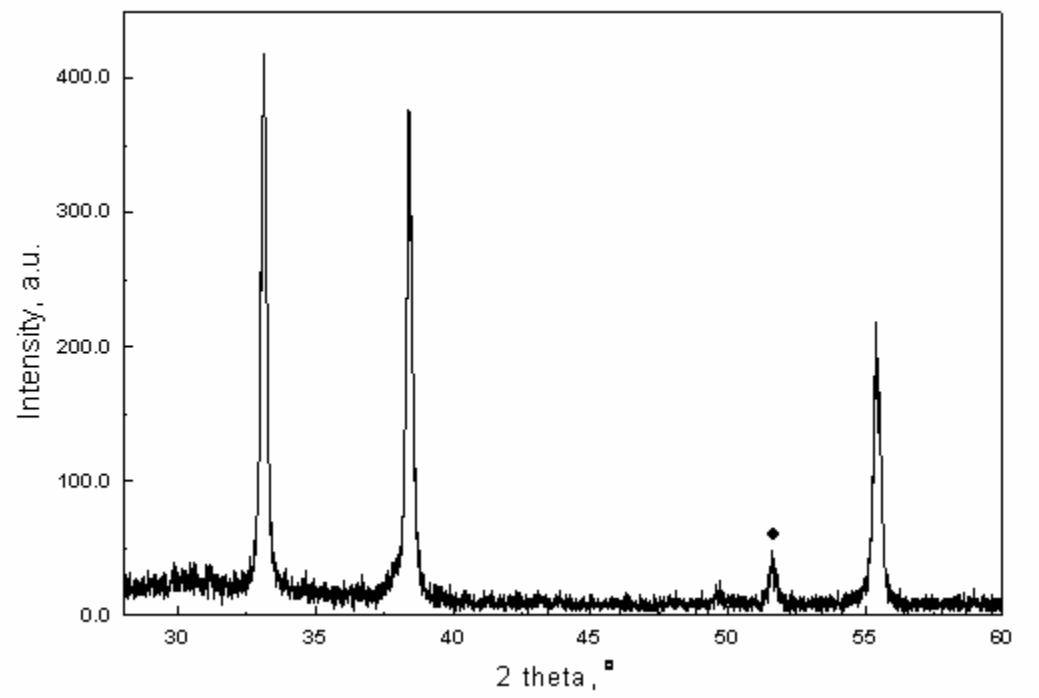

Figure 3.2 A representative X-ray diffractogram of an electrodeposited CdO film.

The grain size of the CdO thin films can be found using the Scherrer formula.[94] The change in grain size manifests in a corresponding broadening of the width of the peaks on the XRD spectrum. Therefore by knowing the width of the X-ray peak at half maximum (in radians) and the wavelength of the X-ray beam used, the size of the particle (D) can be determined using the expression

$$D = \frac{0.89\lambda}{\beta \cos\theta} \text{ Å} \qquad [3.9]$$

where,

$\lambda -$ wavelength of copper Kα = 1.5405 Å

$\beta -$ full width at half maximum (in radians)

$\theta -$ diffraction angle

The mean crystallite size calculated from the Scherrer formula[94] is listed in Table 3.2.

Table 3.2 Grain sizes of an electrodeposited CdO film at different orientations.

	Grain size, nm
(111)	59
(200)	55
(220)	58

Figure 3.3 contains a representative SEM picture of an electrodeposited CdO sample similar to that considered above. A cauliflower-type morphology is seen with uniform coverage of the substrate as also observed in previous studies for CdO films deposited by spray pyrolysis[25] and sol-gel[31] processes respectively.

Auger electron spectra of the CdO film samples after thermal anneal revealed signals from the ubiquitous C at 271.25 eV (KLL transition) along with the expected signals for Cd at 321.05 eV and 378.67 eV (MNN) and O at 513.44 eV (KLL). Smaller signals from the substrate were also observed for Sn (MNN) at 431.41 eV and from the electrolyte for Cl LMM at 180. 43 eV. Quantitative analysis of the Cd and O signal yielded a Cd:O atom ratio of 53:47. It was found that the Cd:O ratio in the film increased marginally with depth implying that the crystallites in the bulk of the film possessed defects such as metal interstitials and O_2 deficiencies. This is expected and is the reason for the high conductivity in CdO.

The optical band gap of the material was determined from a transmittance (% T) vs. wavelength (λ) plot. The fundamental absorption, which corresponds to electron excitation from the valence band to conduction band, can be used to determine the nature and value of the optical band gap. The relation between the absorption coefficient (α) and the incident photon energy (hν) can be written as

$$\alpha = \frac{A(h\upsilon - E_g)^n}{h\upsilon} \qquad [3.10]$$

In Eqn. 3.10, α is the absorption coefficient, A is a constant, the exponent, n = ½ for an

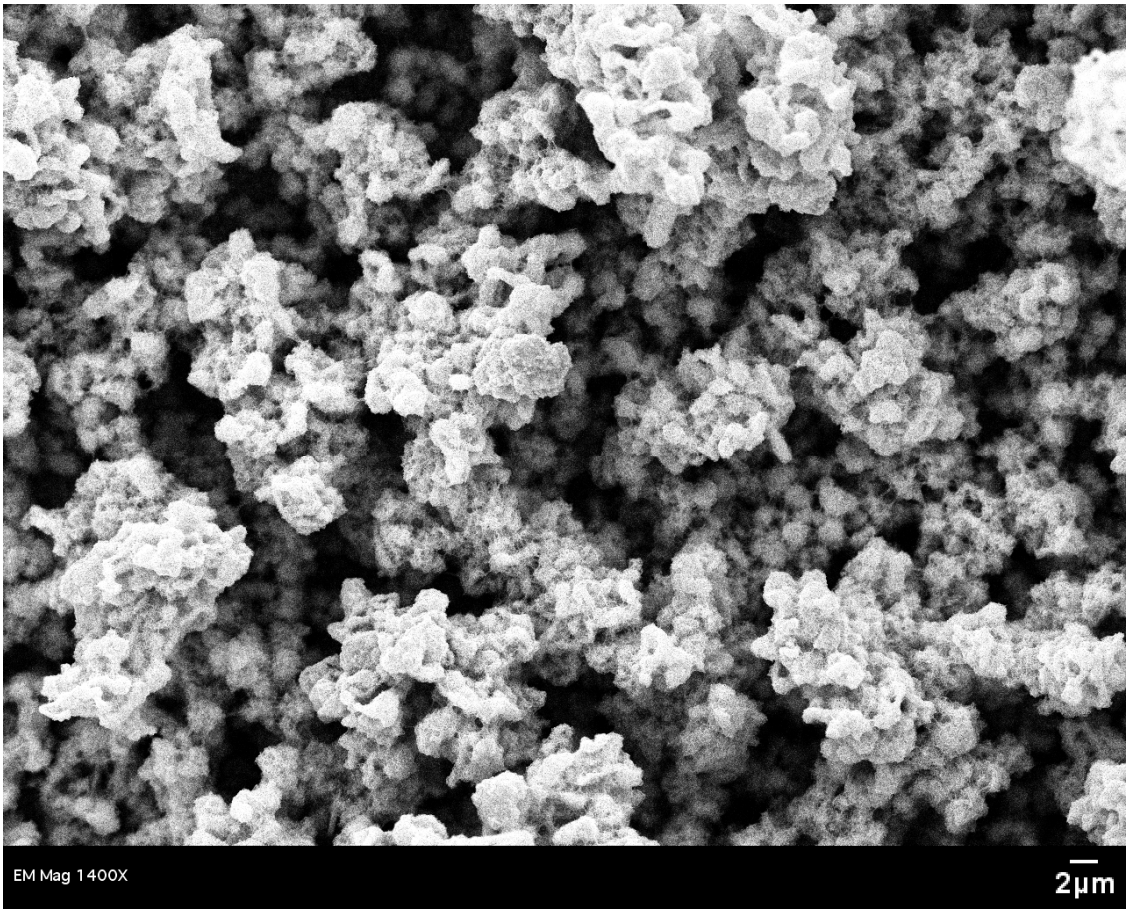

Figure 3.3 SEM picture showing the morphology of an electrodeposited CdO film.

allowed direct transition and the other symbols have their usual meaning.

The optical transmission spectrum of a CdO film in the 250-850 nm range is shown in Figure 3.4. A plot of $(\alpha h\nu)^2$ vs. $h\nu$ according to Eqn. 3.10 is contained in Figure 3.5. The straight line portion of the plot is extrapolated to the energy axis at $\alpha = 0$ to afford an estimate for the band gap energy, E_g. A value for $E_g = 2.25$ eV is obtained (Figure 3.5). This value is in excellent agreement with that known for CdO

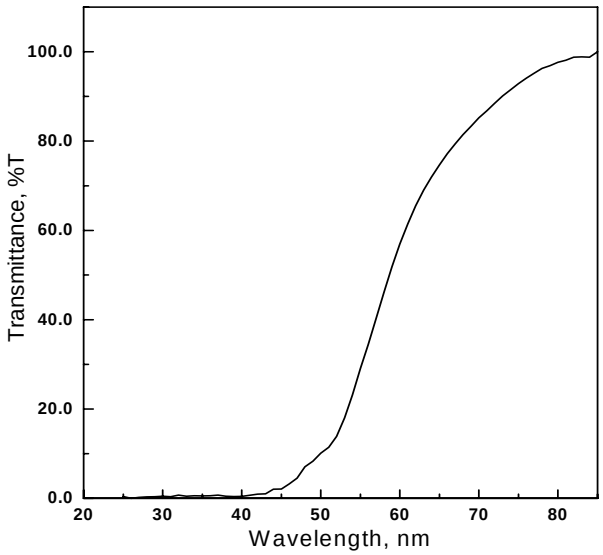

Figure 3.4 Transmittance spectrum for an electrodeposited CdO film.

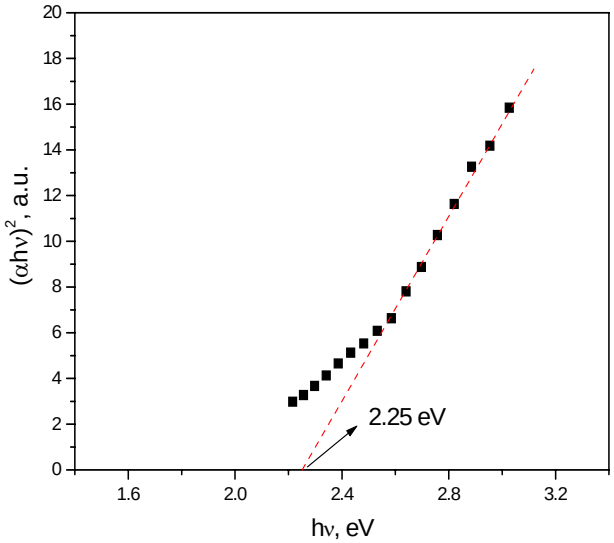

Figure 3.5 Band gap determination for an electrodeposited CdO film.

and is also in line with values measured for CdO film samples prepared by other methods which fall in the 2.2–2.4 eV range. However, it is also noted that the E_g value for CdO is very sensitive to a variety of factors related to the non-stoichiometry of the oxide. Thus the absorption tail observed in the vicinity of the cut-off wavelength (Figure 3.5) is consistent with the presence of defects in the material.

Figure 3.6a contains a photovoltammogram for CdO-coated SnO_2 electrodes in 0.1 M Na_2SO_4 supporting electrolyte. The photocurrents are anodic in polarity consistent with the n-type semiconductor behavior of the electrodeposited CdO film. The dark currents in the reverse bias regime, positive of ~ -0.3 V, are negligible over a reasonably wide potential range (~ 1300 mV). This attests to the non-leaky rectifying nature of the n-CdO/electrolyte interface. An anodic current flow positive of ~ 1.0 V in the "dark" presumably arises from oxidation the film itself. Similarly, the fate of thephotogenerated holes (giving rise to the photocurrent spikes in Figure 3.6a was not explored. However, these photocurrents at moderate reverse bias potentials are entirely stable over a time span of several minutes as diagnosed by the transient photocurrent data in Figure 3.6b.

In summary of the results presented in this section, CdO thin films were electrodeposited on SnO_2 substrates using the cathodic base electrogeneration approach in an aqueous medium containing Cd^{2+} species and dissolved O_2.

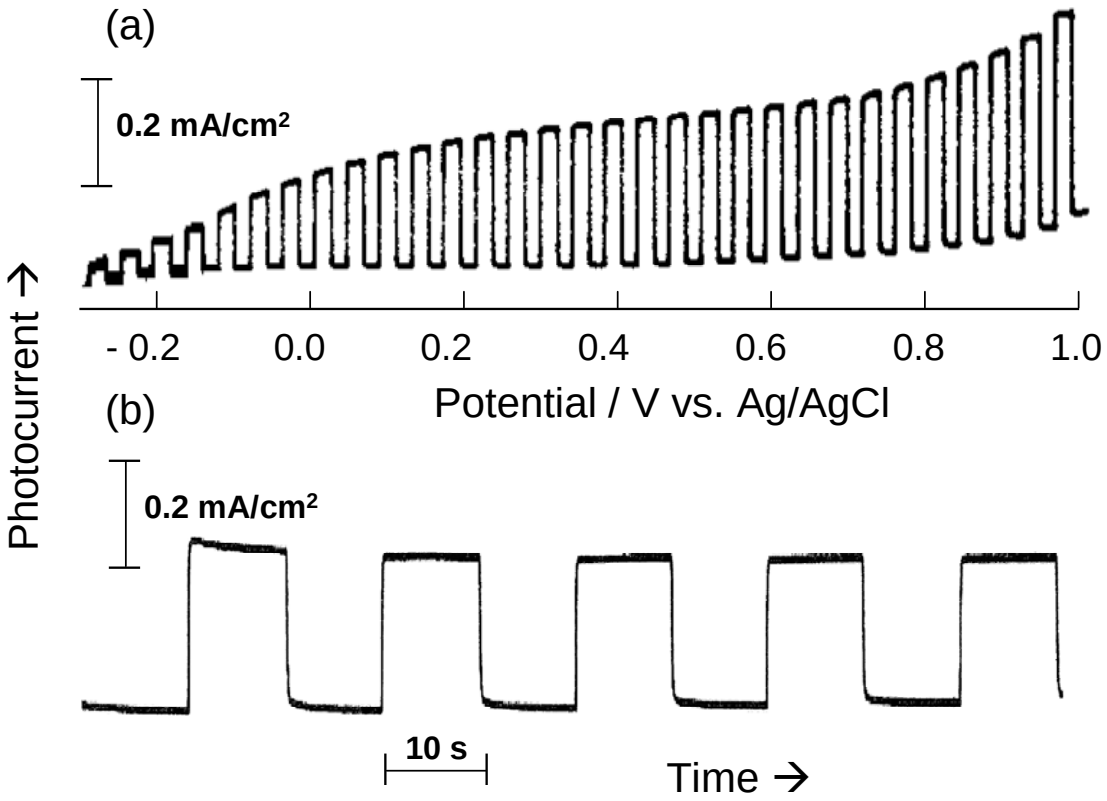

Figure 3.6 A photovoltammogram at 0.1 Hz chopped irradiation (a) and transient photocurrent profile (b) for a CdO film 0.1 M Na_2SO_4. The film was electrodeposited on a TCO substrate. Photovoltammograms were obtained at 2 mV/s; the full output of 100 W tungsten-halogen lamp was used in both sets of experiments. The transients in Figure 3.6 (b) were measured at 0.70 V.

3.2 Zinc Oxide

The voltammetry was carried out in 0.1 M KCl solution (supporting electrolyte) at 80 ^{0}C. The conditions under which the studies were carried out are detailed below.

a) Scan with N_2 purge / O_2 purge (in the absence of Zn^{2+})

The control scan with N_2 purge through the supporting electrolyte and without Zn^{2+} species present was flat with near zero current and featureless and is not shown. The dissolved oxygen present in the solution undergoes reduction at about -400 mV, giving rise to a reduction wave under diffusion control at more negative potentials. The electrogeneration of the base that occurs under this condition is similar to the one shown earlier for CdO deposition.

$$\tfrac{1}{2}\, O_2 + H_2O + 2\, e^- \rightarrow 2\, OH^- \qquad [3.1]$$

b) Scan with Zn^{2+} species in solution (in the absence of dissolved O_2)

In the presence of Zn^{2+} and N_2 we see a large cathodic wave during the forward scan with onset at -1050 mV. The deposited zinc is reoxidized to form Zn^{2+}on the reverse scan. The reactions corresponding to this scan are (Figure 3.7):

$$Zn^{2+} + 2e^- \rightarrow Zn \qquad [3.12]$$

$$Zn \rightarrow Zn^{2+} + 2e^- \qquad [3.13]$$

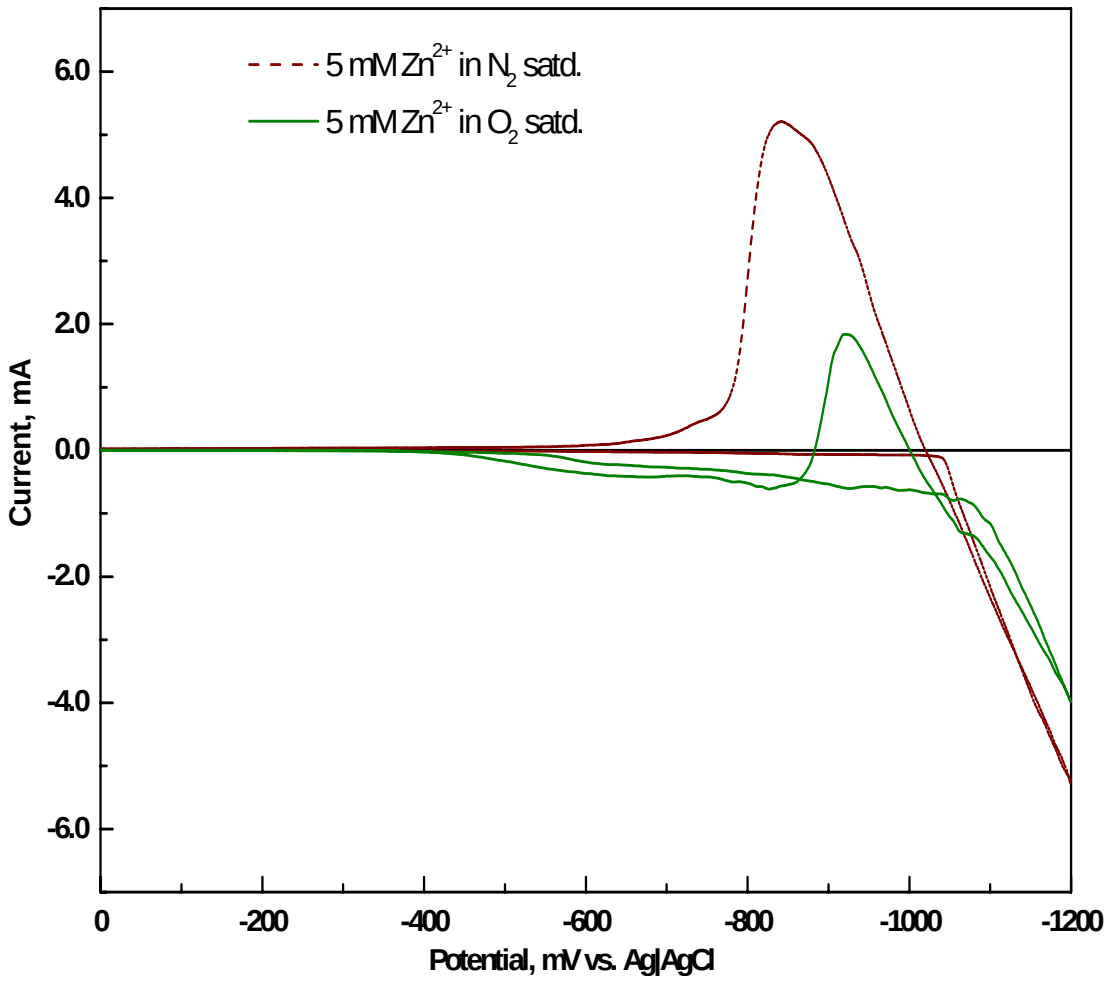

Figure 3.7 Cyclic voltammograms for a TCO electrode in two solutions as shown. The supporting electrolyte was 0.1 M KCl.

c) Scan with Zn^{2+} and O_2 in solution

In the presence of O_2 and Zn^{2+} species in solution, we see a cathodic wave onset at -400 mV, this coincides with the reduction of oxygen which is essential for the deposition of zinc oxide. The deposition of zinc oxide or hydroxide (an alternate reaction) begins at this potential and continues to takes place until -1100 mV, at which juncture, zinc metal is deposited. Note that the deposition potential for metallic zinc shifts to a more negative value in the presence of oxygen. The reverse scan shows a much lower anodic current at -1000 mV which is a net current generated by the combination of reduction and oxidation reactions taking place at this potential.

To summarize, the method to produce zinc oxide films consists of generating hydroxide ions at the surface of an electrode by cathodically reducing an oxygen precursor (generation of OH^-) as in the CdO case discussed earlier. This process leads to a pH increase in the vicinity of the electrode and a local supersaturation for zinc oxide precipitation which provokes the formation of zinc oxide films on the electrode surface[85].

The reaction mechanism can be summarized as:

$$\tfrac{1}{2}\, O_2 + H_2O + 2e^- \rightarrow 2OH^- \qquad [3.1]$$

$$Zn^{2+} + 2OH^- \rightarrow ZnO + H_2O \qquad [3.14]$$

$$Zn^{2+} + \tfrac{1}{2}\, O_2 + 2e^- \rightarrow ZnO \qquad [3.15]$$

The alternative to the above reaction is the formation of zinc hydroxide which is annealed to form ZnO.

$$Zn^{2+} + 2OH^- \rightarrow Zn(OH)_2 \qquad [3.16]$$

$$Zn(OH)_2 \xrightarrow{\Delta} ZnO + H_2O \qquad [3.17]$$

The above experiments helped determine the optimal deposition potential to be -950 mV, which is at a potential negative enough for improved deposition rates but low enough to make sure there is no zinc metal formation.

X–ray diffractograms of ZnO films deposited at various temperatures (50 ^{0}C, 65 ^{0}C, 80 ^{0}C, and 90 ^{0}C) are shown in Figure 3.8. All the films were deposited at a potential of -950 mV and 5 mM zinc chloride concentration in solution. The anneal temperature was 500 ^{0}C. The XRD patterns of the polycrystalline films formed reveal a hexagonal structure corresponding to the reference pattern for ZnO[95]. The films deposited show an increase in orientation with an increase in the deposition bath temperature. At 50 ^{0}C the intensities of the (101) and the (002) planes are about the same. An increase in relative intensity and the narrowing of the peak width are seen with an increase in the deposition temperature. This indicates improved preferred orientation and formation of larger grains. As before, the grain size of the ZnO thin films can be found using the Scherrer formula (Eqn. 3.9). Figure 3.9 contains a plot of the crystallite sizes versus electrodeposition temperature for the data in Table 3.3. It is

seen that with increasing temperature the ZnO grains are more elongated along the C-axis and reaches a maximum at 80 ^{0}C.

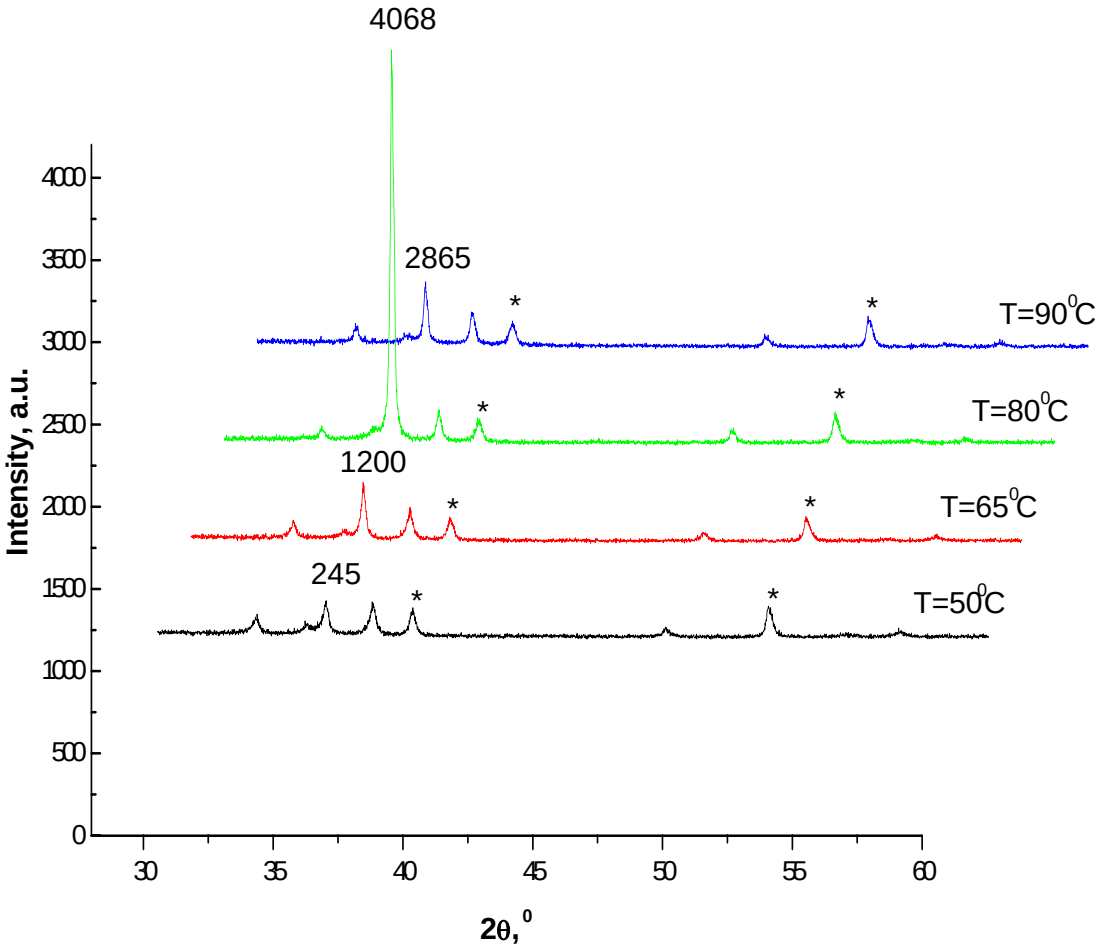

Figure 3.8 X-ray diffractograms of ZnO films electrodeposited at different deposition temperatures.

Table 3.3 Variation of grain size of ZnO thin films electrodeposited at different temperatures.

	(T = 50 ^{0}C)	(T = 65^{0}C)	(T = 80 ^{0}C)	(T = 90 ^{0}C)
(100)	34.6	28.7	28.3	33.4
(002)	27.3	36.5	46.1	38.5
(101)	30.6	34.9	35.8	32.8

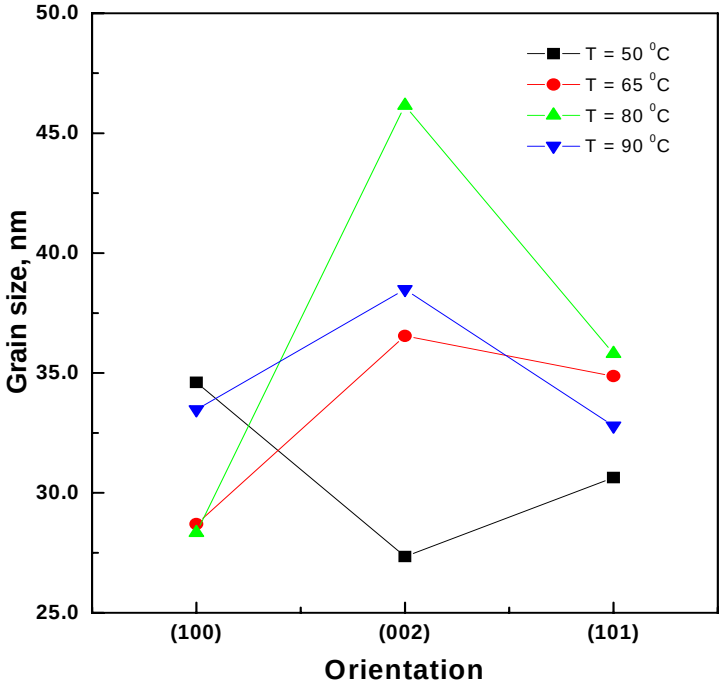

Figure 3.9 Plots of the ZnO grain size data shown in Table 3.3.

The film morphology was observed by SEM. The films were ~1 μm thick and were the same ones on which X-ray diffraction studies were carried out. Films deposited at 50 ^{0}C (Figure 3.10), possess a structure which looks flaky, with a number of thin petal-like shapes arranged in random order. As the deposition temperature is increased to 65 ^{0}C (Figure 3.11) we see an improved order and crystalinity in the film. At 80 ^{0}C (Figure 3.12), we see a separation in the petal-like structure and emergence of pillars amidst the petals. This corresponds to the films with the highest degree of orientation. The films at 90 ^{0}C (Figure 3.13) show a dense film with the pillars reducing in size. Flower-like structures are formed at equally spaced intervals. The film has an appearance of a mosaic of triangular tiles dotted with these flowery growths at the intersections.

The X–ray photoelectron spectroscopy (XPS) studies on the films show a variation in the zinc to oxygen ratio with deposition temperature (Table 3.4). A near 1:1 stoichiometric ratio of zinc and oxygen is seen in the films at lower temperatures (50 ^{0}C and 65 ^{0}C). The film at 80 ^{0}C shows an increase in the percentage of oxygen content, which is further increased at 90 ^{0}C. The reason(s) for these compositional trends are not clear at present. We also see about 1.5 % chlorine in the films deposited upto 80 ^{0}C. The chlorine content reduces to 0.7 % at 90 ^{0}C.

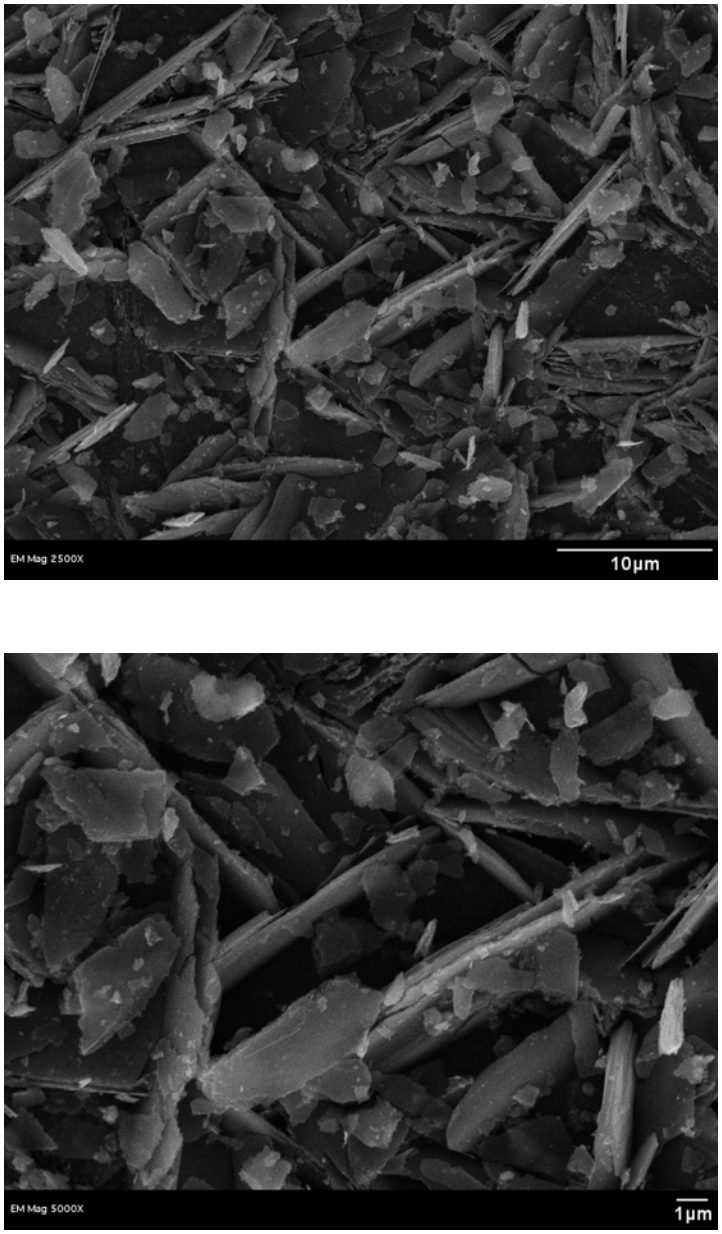

Figure 3.10 SEM pictures of ZnO films electrodeposited at 50 ^{0}C shown at different magnifications, (top) 2500X, (bottom) 5000X.

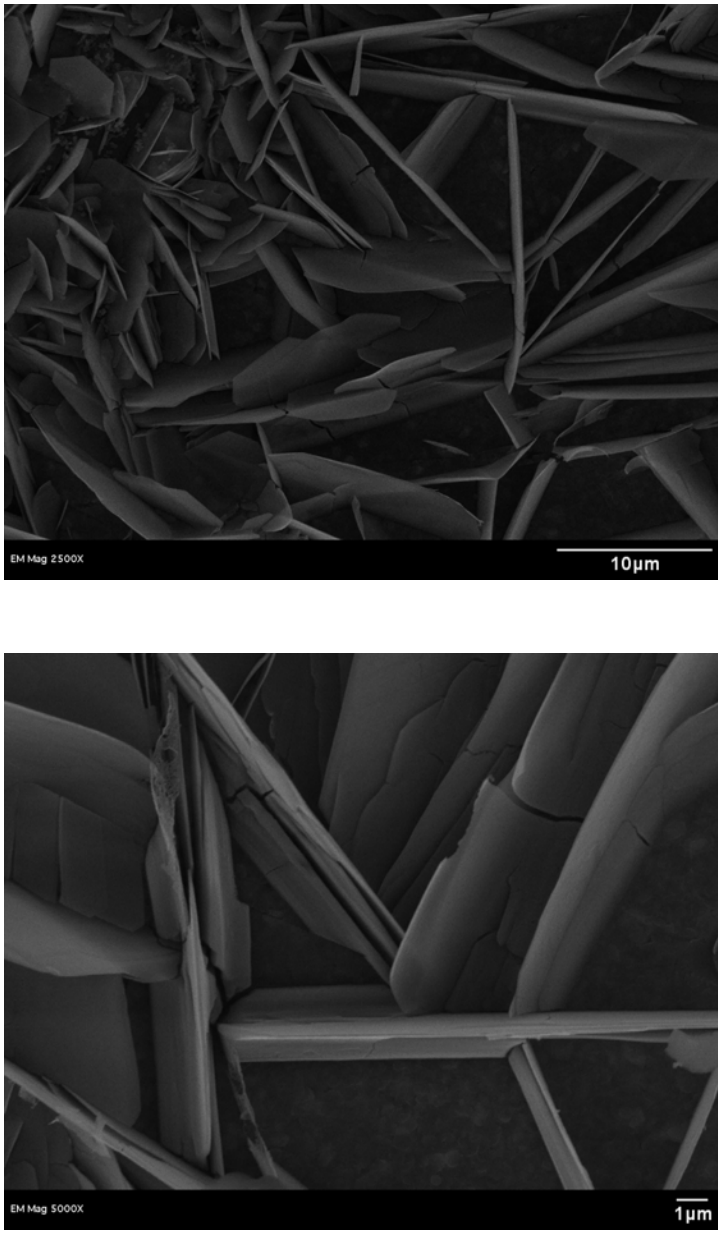

Figure 3.11 SEM pictures of ZnO films electrodeposited at 65 ^{0}C shown at different magnifications, (top) at 2500X, (bottom) 5000X.

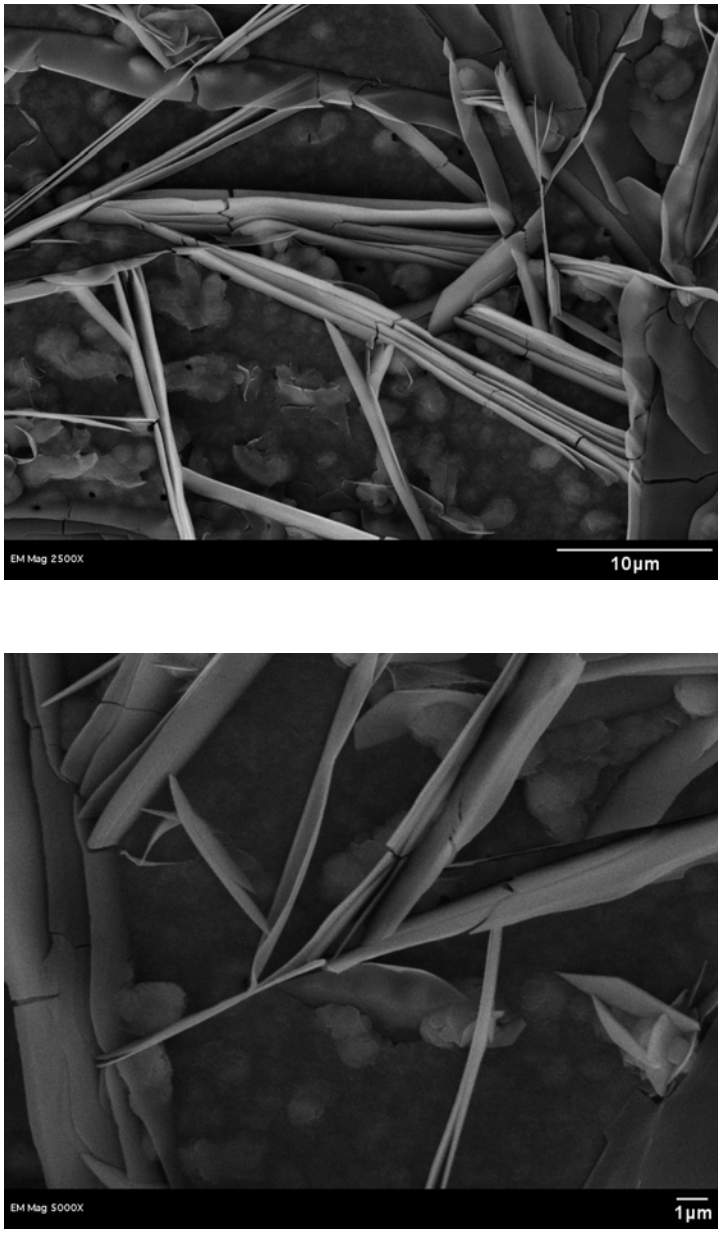

Figure 3.12 SEM pictures of ZnO films electrodeposited at 80 ^{0}C shown at different magnifications, (top) 2500X, (bottom) 5000X.

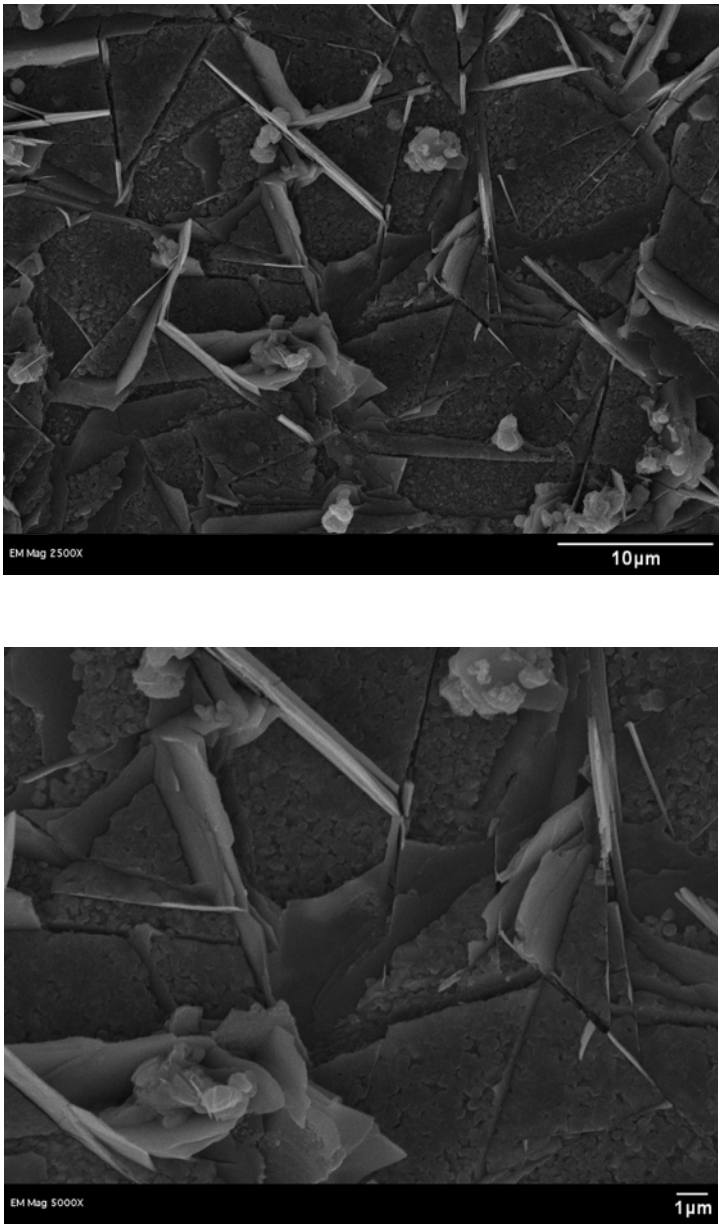

Figure 3.13 SEM pictures of ZnO films electrodeposited at 90 ^{0}C shown at different magnifications, (top) 2500X, (bottom) 5000X.

Table 3.4 XPS data showing the zinc: oxygen: chlorine ratio in the samples deposited at different temperatures.

	(T = 50 ^{0}C)	**(T = 65 ^{0}C)**	**(T = 80 ^{0}C)**	**(T = 90 ^{0}C)**
Zn	44.5	44.9	43.7	37.1
O	47.5	47.3	50.7	57.6
Cl	1.5	1.7	1.7	0.7

The optical transmission spectrum of a (001) oriented ZnO film in the 250-850 nm range is shown in Figure 3.14. A plot of $(\alpha h\nu)^2$ vs. $h\nu$ according to Eqn. 3.10. is shown in Figure 3.15. The straight line portion of the plot is extrapolated to the energy axis at $\alpha = 0$ to afford an estimate for E_g. A value for $E_g = 3.3$ eV is obtained (Figure 3.15). This value is in excellent agreement with that known for ZnO and is also in line with values measured for ZnO film samples prepared by other methods which fall in the 3.1 – 3.5 eV range.

In summary of the results presented in this section, ZnO thin films were electrodeposited on SnO_2 substrates using the cathodic base electrogeneration approach in an aqueous media containing Zn^{2+} species and dissolved O_2. The ZnO films were successfully electrodeposited with a preferred orientation along the c-axis. These studies were conducted as a prelude to the $(CdO)_x(ZnO)_{1-x}$, mixed oxide film deposition which will be described in the next section.

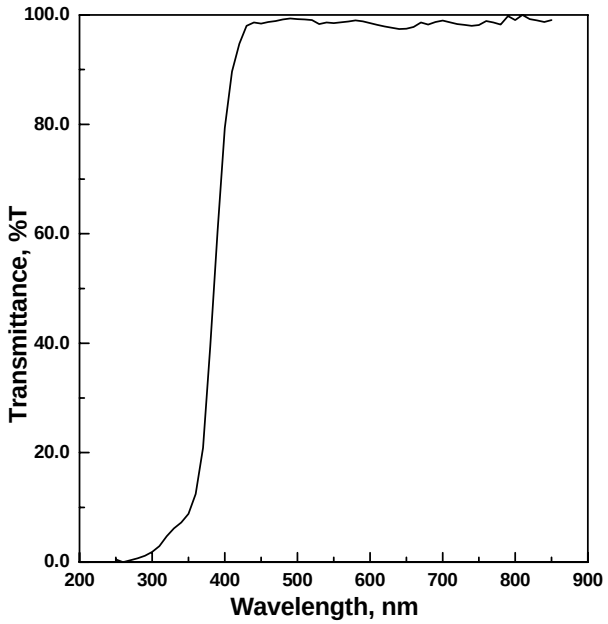

Figure 3.14 Transmittance spectrum for an electrodeposited ZnO film.

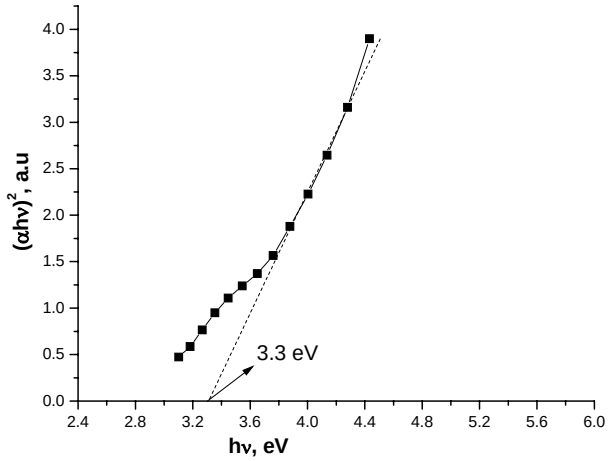

Figure 3.15 Band gap determination for an electrodeposited ZnO film.

3.3 Mixed Cadmium Oxide-Zinc Oxide

The first study on the "base electrogeneration" strategy for preparing $(CdO)_x$ $(ZnO)_{1-x}$ thin films by cathodic electrodeposition from aqueous media is presented below. The mechanistic aspects of the film deposition process are briefly explored along with characterization of the deposited material by X-ray diffraction, scanning electron microscopy, and surface analysis techniques. Finally, the photoelectrochemical behavior of the deposited material is presented.

Figure 3.16 contains cyclic voltammograms for the TCO working electrode in 0.1 M KCl supporting electrolyte. Two solution conditions are considered and in both cases the scan was begun at 0 V in the negative direction upto the switch limit of -1.0 V and back to 0 V. The control scan with N_2 purge in the absence of Cd^{2+} and Zn^{2+} in solution is similar to the result shown in Figure 3.1 and is as per Eqn. 3.1. The conditions specific to $(CdO)_x(ZnO)_{1-x}$ electrodeposition were studied in a bath which contained 1 mM cadmium chloride and 4 mM zinc chloride in solution. The results from these studies are presented below.

a) Scan with Cd^{2+} and Zn^{2+} in solution (in the absence of dissolved O_2)

The forward scan with Cd^{2+} and Zn^{2+} species in solution (Figure 3.16) is similar to the scan with only Cd^{2+} in solution (Figure 3.1). The scan shows a cathodic current onset at ~ -760 mV, which corresponds to the deposition of cadmium metal (Eqn. 3.2). The return scan does not track the forward scan and an anodic curve follows with a peak at ~ -600 mV, which is assigned to the stripping of cadmium. This anodic current

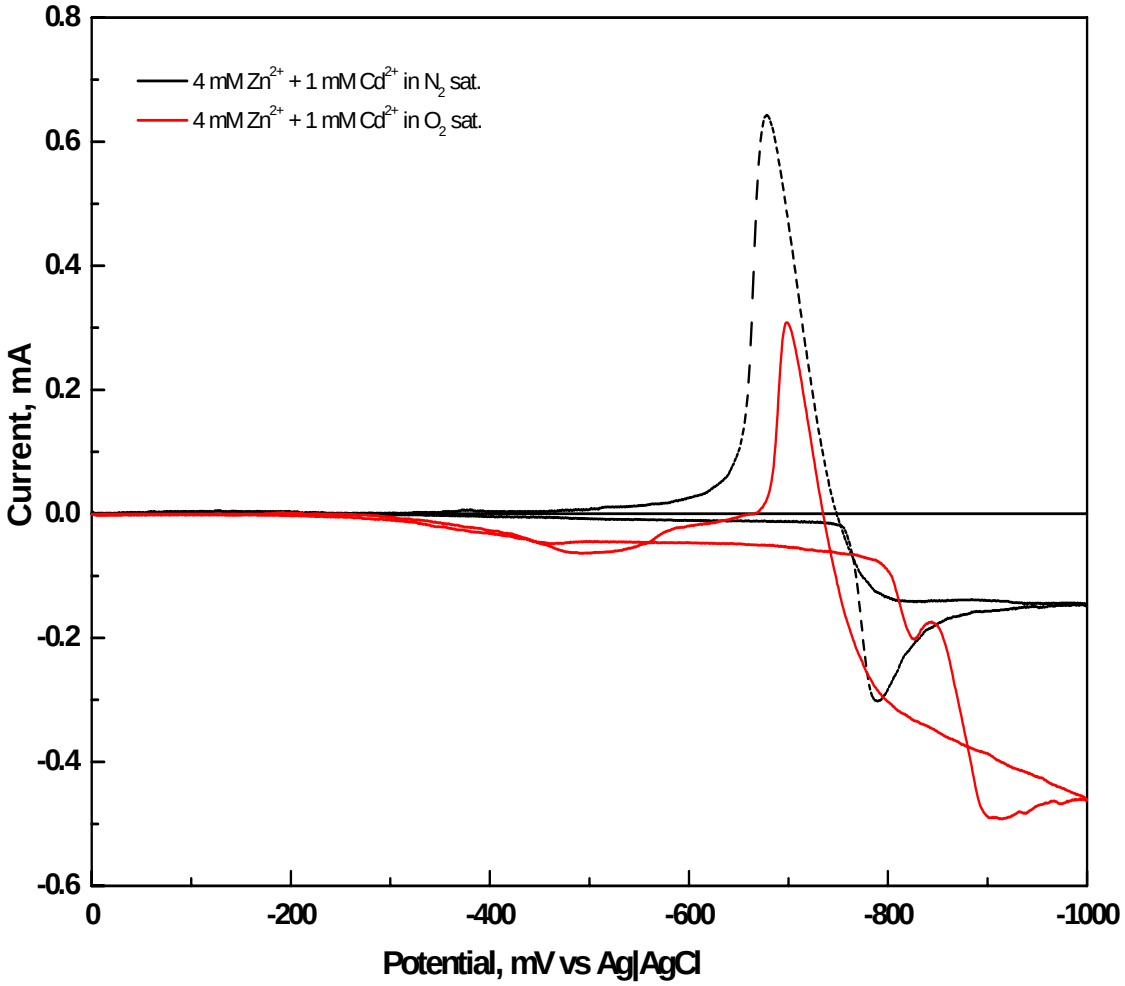

Figure 3.16 Cyclic voltammogram for a TCO electrode in two solutions shown. The supporting electrolyte was 0.1 M KCl.

maximum measures ~ 0.8 mA which is ~2.5 times lower compared to a similar curve (Figure 3.1, 2.5 mM Cd^{2+} in solution). This is due to the reduced amount Cd^{2+} in solution and confirms that Cd deposition (Eqn. 3.2) is the only reaction that takes place at this potential range and that the presence of Zn^{2+} does not influence the reaction.

b) Scan with Cd^{2+}, Zn^{2+}, and O_2 in solution

The second cyclic voltammogram in Figure 3.16 pertains to the case when both Cd^{2+} and Zn^{2+} species as well as dissolved O_2 are present in the supporting electrolyte. The forward scan shows a shift in the Cd deposition wave to a more negative potential of ~ -800 mV, as seen earlier (Figure 3.1). The curve which was considerably suppressed in the presence of Cd^{2+} and O_2 follows the expected path until ~ -820 mV where it takes a sharp downward plunge (large cathodic current). Supplemental ZnO deposition would contribute only minimally to the unexpected surge in the cathodic current. We speculate that the catalyzing effect that Cd^{2+} has on the deposition of ZnO and that Zn^{2+} has on Cd and CdO formation is the main contributing factor for this surge. The enhancement induced by Cd^{2+} on the deposition of ZnO is observed to be a lot more than that of Zn^{2+} on the formation of Cd and CdO.

A number of reactions, as discussed earlier under ZnO and CdO film formation, are possible in this potential range and are listed below:

$$Cd^{2+} + 2OH^- \rightarrow CdO + H_2O \qquad [3.4]$$

$$Cd^{2+} + \tfrac{1}{2} O_2 + 2e^- \rightarrow CdO \qquad [3.5]$$

$Cd^{2+} + 2OH^- \rightarrow Cd(OH)_2$ [3.6]

$Zn^{2+} + 2OH^- \rightarrow ZnO + H_2O$ [3.14]

$Zn^{2+} + ½O_2 + 2e^- \rightarrow ZnO$ [3.15]

$Zn^{2+} + 2OH^- \rightarrow Zn(OH)_2$ [3.16]

The products of Eqn. 3.6 and Eqn. 3.16 are converted to their respective oxides (Eqn. 3.7 and Eqn. 3.17) during the post-deposition anneal carried out at 450 ^{0}C.

$Cd(OH)_2 \xrightarrow{\Delta} CdO + H_2O$ [3.7]

$Zn(OH)_2 \xrightarrow{\Delta} ZnO + H_2O$ [3.17]

For ex situ analyses, films were potentiostatically deposited at – 950 mV at 80 ^{0}C for 15 minutes. These films were deposited from electrodeposition baths with different Zn^{2+} to Cd^{2+} ratios as mentioned earlier (Chapter 2).

Figure 3.17 contains representative XRD patterns for electrodeposited $(CdO)_x(ZnO)_{1-x}$ films treated as above. When there is an equal amount of Zn^{2+} and Cd^{2+} species in solution (50:50), the reflections which belong to the CdO component in the film are dominant. Under these deposition conditions the amount of ZnO in the film is very small. This is evident from the low intensity of the ZnO reflections seen the diffraction plots. The ZnO reflections are enhanced in size as the ratio of Zn^{2+} to Cd^{2+} in solution increases (Figure 3.17) and reach a point at which the intensity of the ZnO and CdO peaks are nearly equal corresponding to a Zn^{2+}:Cd^{2+} ratio in solution of 90:10. Additionally, two peaks assignable to the SnO_2 substrate are also seen.

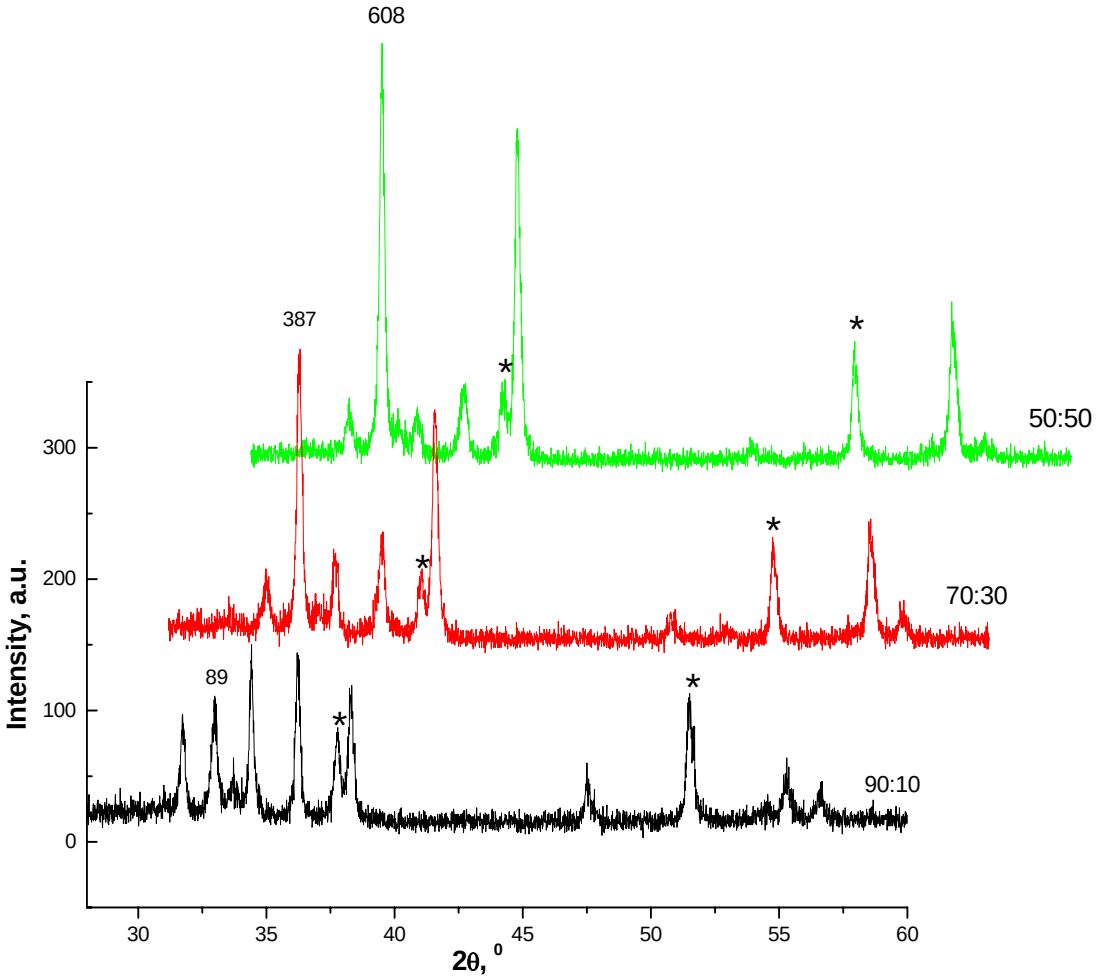

Figure 3.17 X-ray diffractograms of $(CdO)_x(ZnO)_{1-x}$ films electrodeposited from solution with different concentrations of Zn^{2+}:Cd^{2+} species as shown.

The XPS analysis of the films shows a large excess of Cd (Table 3.5) when an equal amount of Zn^{2+} and Cd^{2+} are present in solution (as expected). At this potential, rapid deposition of CdO takes place and films with more even stoichiometry are seen as the ratio of Zn^{2+}: Cd^{2+} in solution is increased (Table 3.5).

Table 3.5 XPS data showing the zinc: cadmium ratio in films electrodeposited from solution with different concentrations of Zn^{2+}:Cd^{2+}

Zn^{2+}:Cd^{2+} species in solution	Zn:Cd ratio in the film
90:10	41:59
70:30	11:89
50:50	4:96

The SEM pictures (Figures 3.18-3.20) of the films deposited show that the petal-like morphology of ZnO and the cauliflower like morphology of CdO films co-exist at higher ratios of Zn^{2+}:Cd^{2+} species in solution. As this ratio is decreased toward equal amounts of $Zn^{2+}$and Cd^{2+} in solution, the morphology of the films becomes similar to that of CdO, although not as porous as the pure CdO films. We also see that large agglomerates of CdO are formed on the surface when the films are prepared from equal amounts of Zn^{2+} and Cd^{2+} (50:50) species in solution.

The transmittance spectra for the films with varying amounts of Zn^{2+} and Cd^{2+} in the films are shown in Figure 3.21. The spectra show a large variation in the percentage transmittance cut-off from ~ 350 nm (for ZnO) to ~650 nm (for CdO with a small amount, 4%, of ZnO). We find that the mixed oxide films have a separate distinct transmittance spectra which is shifted depending on the amounts of ZnO and CdO in the film. The transmittance spectrum of the film with a ratio 41:59 (Zn^{2+}: Cd^{2+} in the film), shows a shift towards the shorter wavelength (with respect to pure CdO), as expected. The films with 11:89 and 4:96 show a shift in the transmittance spectra towards the

longer wavelength region (with respect to pure CdO). This can be attributed to the non-stoichiometry in the CdO film due to alloying with ZnO. Further studies are planned to tune the band gap of the films by varying the concentration of Zn^{2+}:Cd^{2+} species in solution.

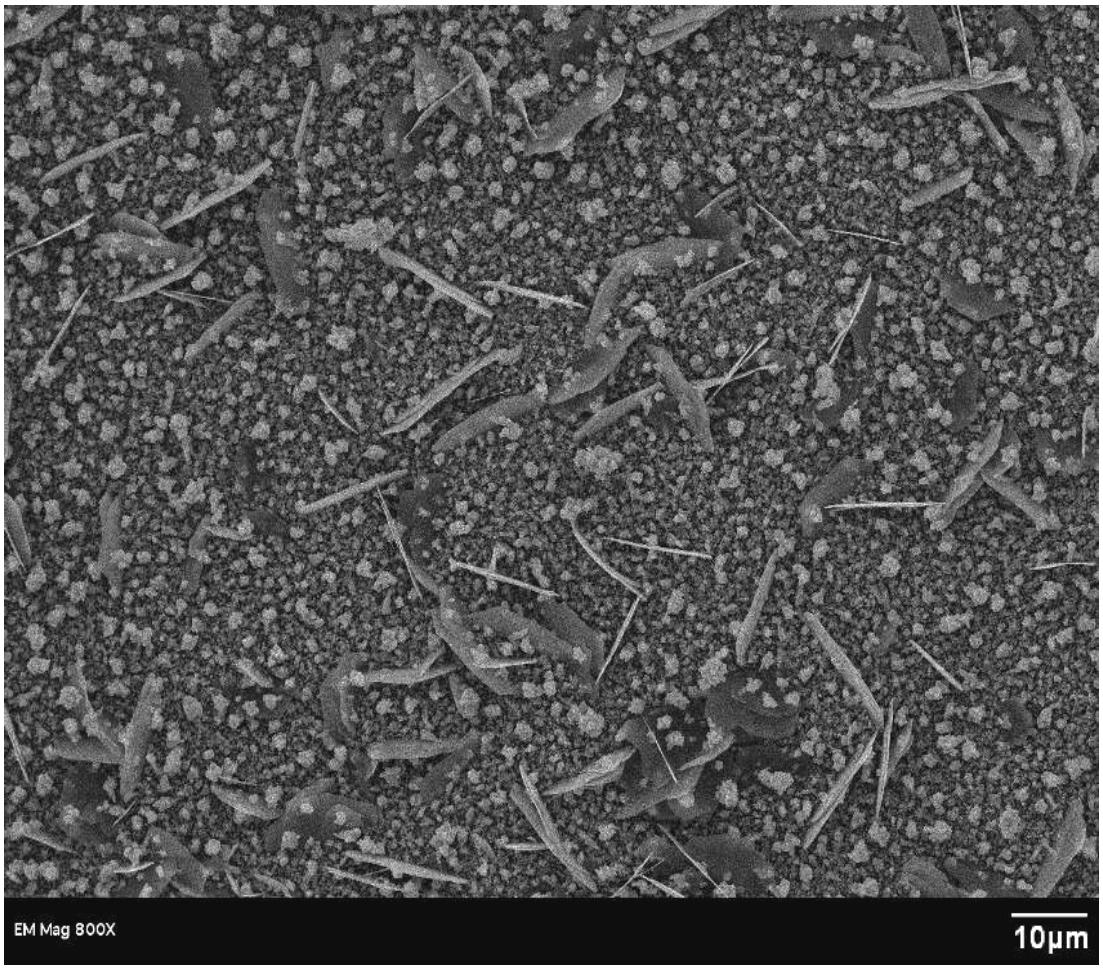

Figure 3.18 SEM picture of a $(CdO)_x(ZnO)_{1-x}$ film electrodeposited from a bath containing $Zn^{2+}$and Cd^{2+} species at a ratio of 90:10.

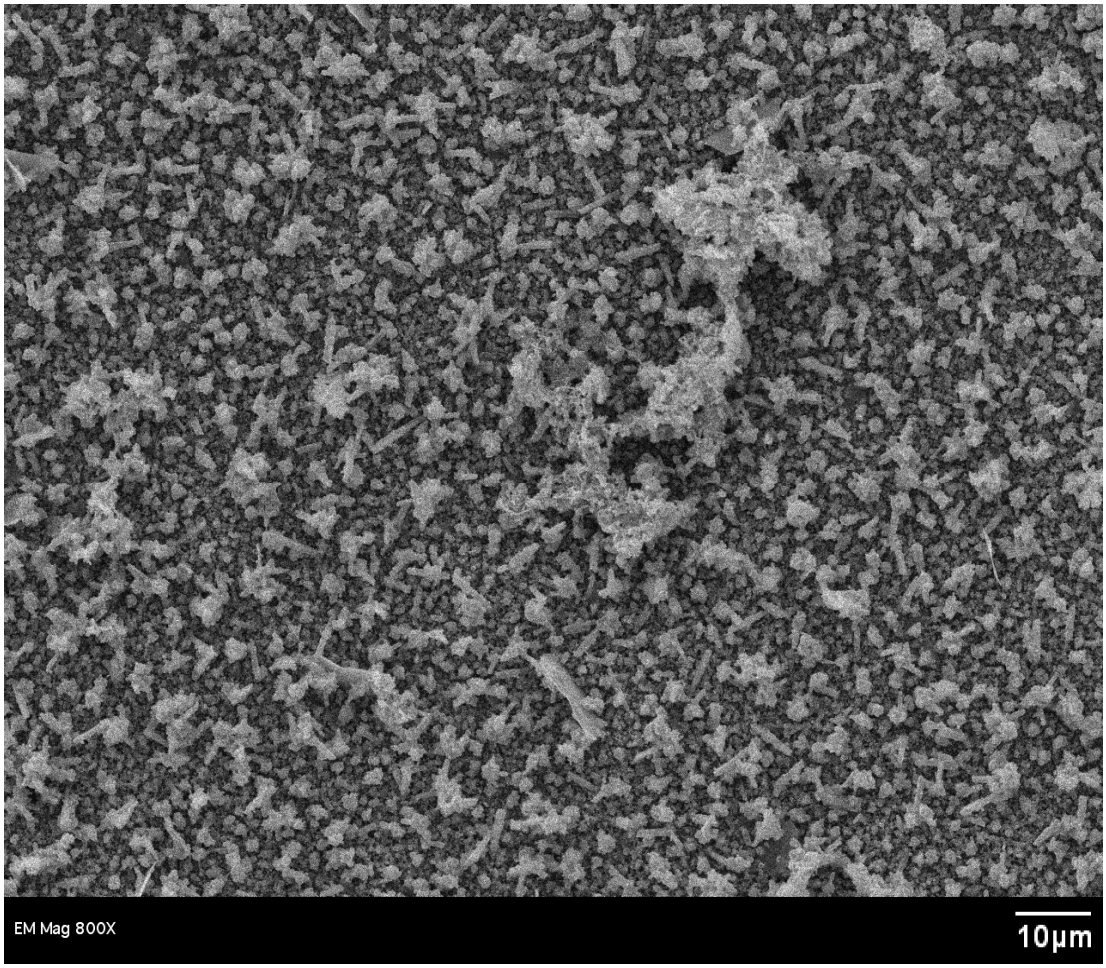

Figure 3.19 SEM picture of a $(CdO)_x(ZnO)_{1-x}$ film electrodeposited from a bath containing $Zn^{2+}$and Cd^{2+} species at a ratio of 70:30.

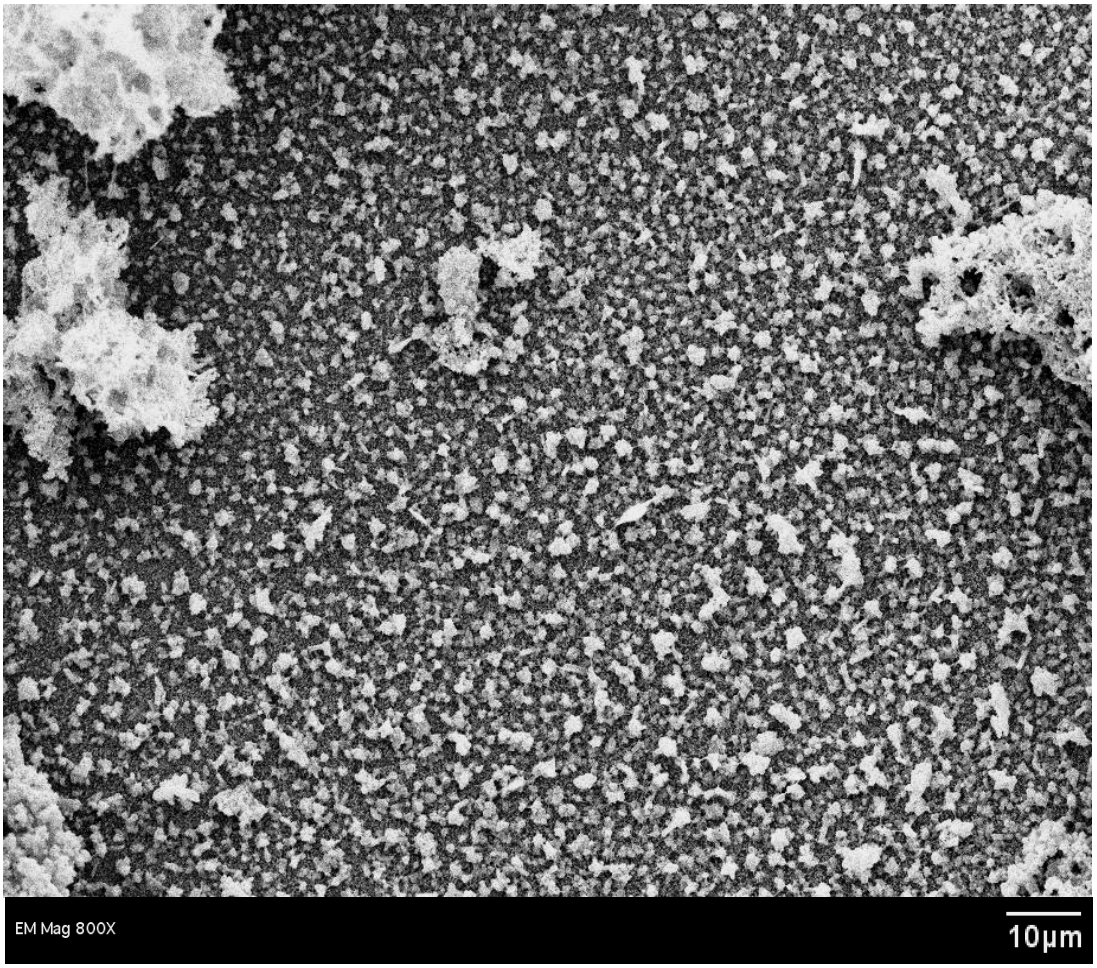

Figure 3.20 SEM picture of a $(CdO)_x(ZnO)_{1-x}$ film electrodeposited from a bath containing $Zn^{2+}$and Cd^{2+} species at a ratio of 50:50.

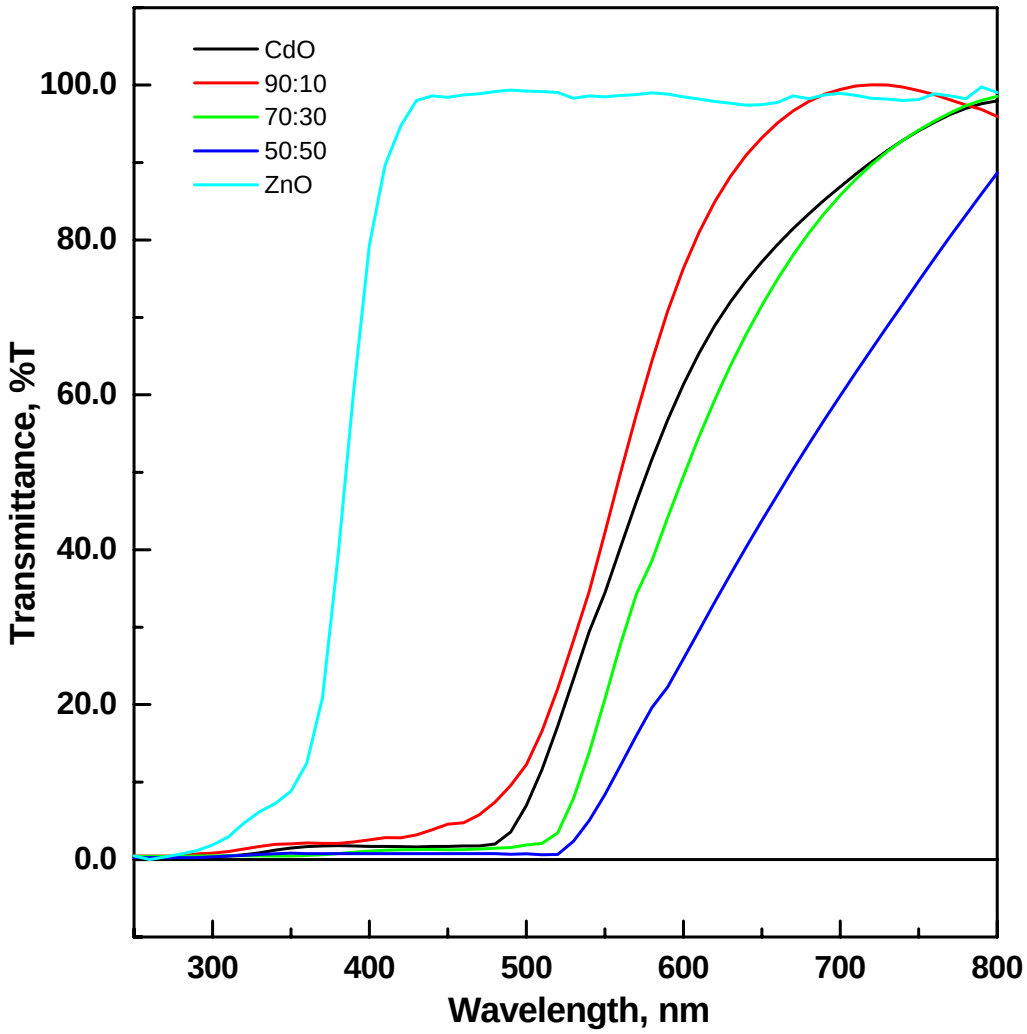

Figure 3.21 Transmittance spectra of electrodeposited $(ZnO)_x(CdO)_{1-x}$ films at The films were deposited from different solution concentrations of Zn^{2+} and Cd^{2+} in solution.

Figure 3.22-3.26 contain photovoltammograms for ZnO, CdO and $(CdO)_x(ZnO)_{1-x}$ coated TCO substrates in 0.1 M Na_2SO_4 supporting electrolyte under UV irradiation. The photocurrents are all anodic in polarity, consistent with the n-type semiconductor behavior of the electrodeposited CdO and ZnO films. The dark currents in the reverse bias regime are negligible over a reasonably wide potential range in all cases. This attests to the non-leaky rectifying nature of the n-$(CdO)_x(ZnO)_{1-x}$/ electrolyte interface.

Figure 3.22a shows a photocurrent profile for ZnO. The measured currents are large (as expected for a wide band gap semiconductor) with a maximum of 500 μA at ~ 0.8 V. However, these photocurrents reduce over a time span of several minutes as evident from the transient photocurrent data in Figure 3.22b**.** The photocurrents measured on CdO films (Figure 3.23a) under similar conditions show a very small but stable photocurrent response (Figure 3.23b). The photocurrent is considerably diminished with respect to the photocurrent associated with CdO films irradiated under visible light (Figure 3.6), which is expected as CdO is photoactive only in the visible region of the electromagnetic spectrum.

The mixed oxide films show a decrease in photoactivity with increase in cadmium content in the films. Though the photocurrents are considerably reduced, we observe that the stability of the photocurrents is very good which legitimizes the alloying of CdO with ZnO. We also see that the shape of the photocurrent profile is influenced by the CdO in the films and the decrease in photocurrent observed before the

onset of the "dark current" (seen in pure ZnO films) is not seen in the alloyed films. (Figures 3.24–3.26).

In summary of the results presented in this section, $(CdO)_x(ZnO)_{1-x}$ thin films were electrodeposited on SnO_2 substrates using the cathodic base electrogeneration approach in an aqueous media containing Zn^{2+}, Cd^{2+} species and dissolved O_2.

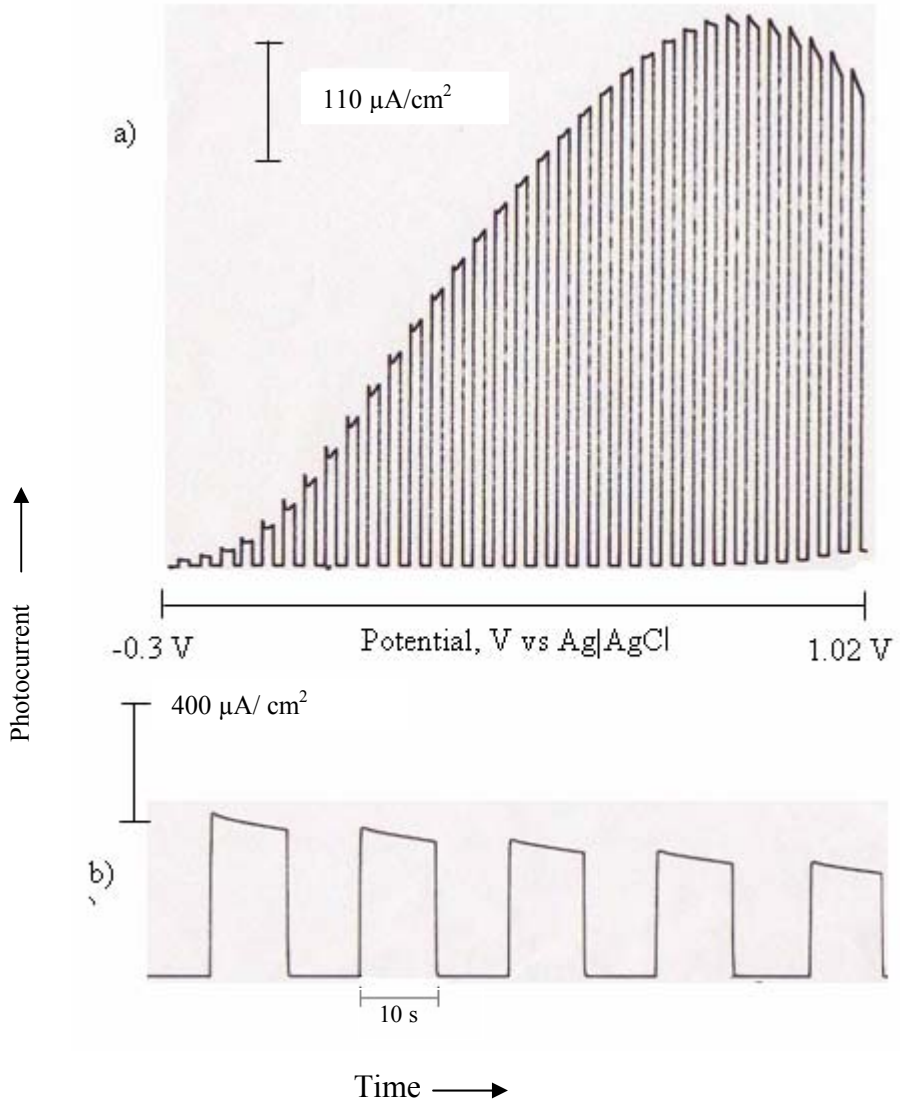

Figure 3.22 A photovoltammogram at 0.1 Hz chopped irradiation (a) and transient photocurrent profile (b) for a ZnO film 0.1 M Na_2SO_4. The film was electrodeposited on a TCO substrate. Photovoltammograms were obtained at 2 mV/s; the full output of 75 W xenon arc lamp was used in both sets of experiments. The transients in Figure 3.22(b) were measured at 0.80 V.

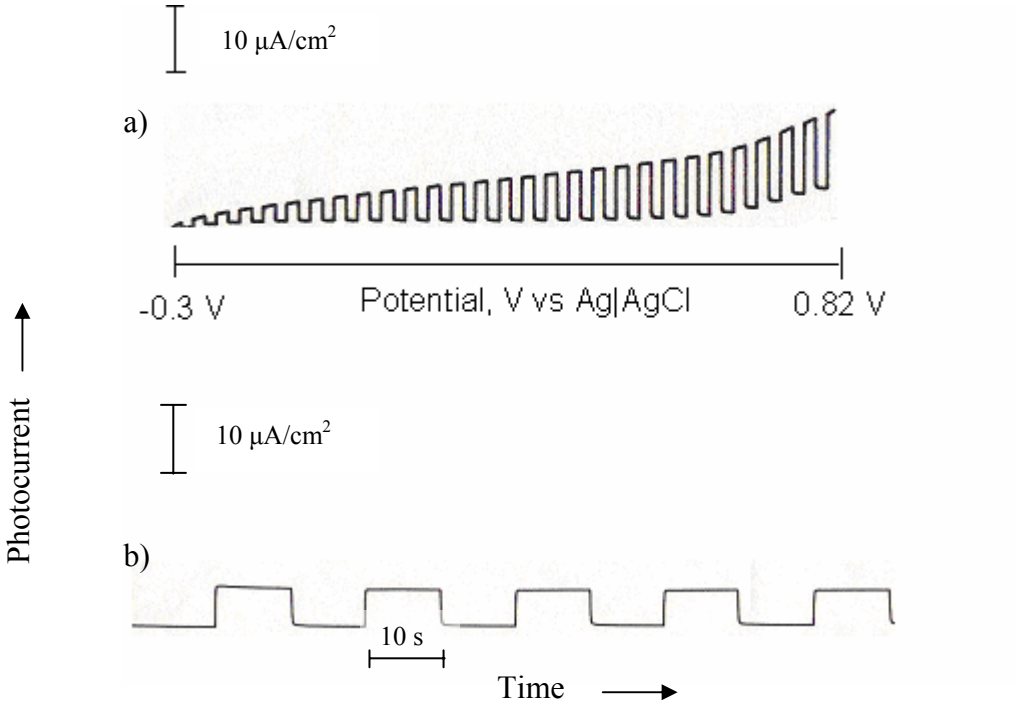

Figure 3.23 A photovoltammogram at 0.1 Hz chopped irradiation (a) and transient photocurrent profile (b) for a CdO film 0.1 M Na_2SO_4. The film was electrodeposited on a TCO substrate. Photovoltammograms were obtained at 2 mV/s; the full output of 75 W xenon arc lamp was used in both sets of experiments. The transients in Figure 3.23(b) were measured at 0.70 V.

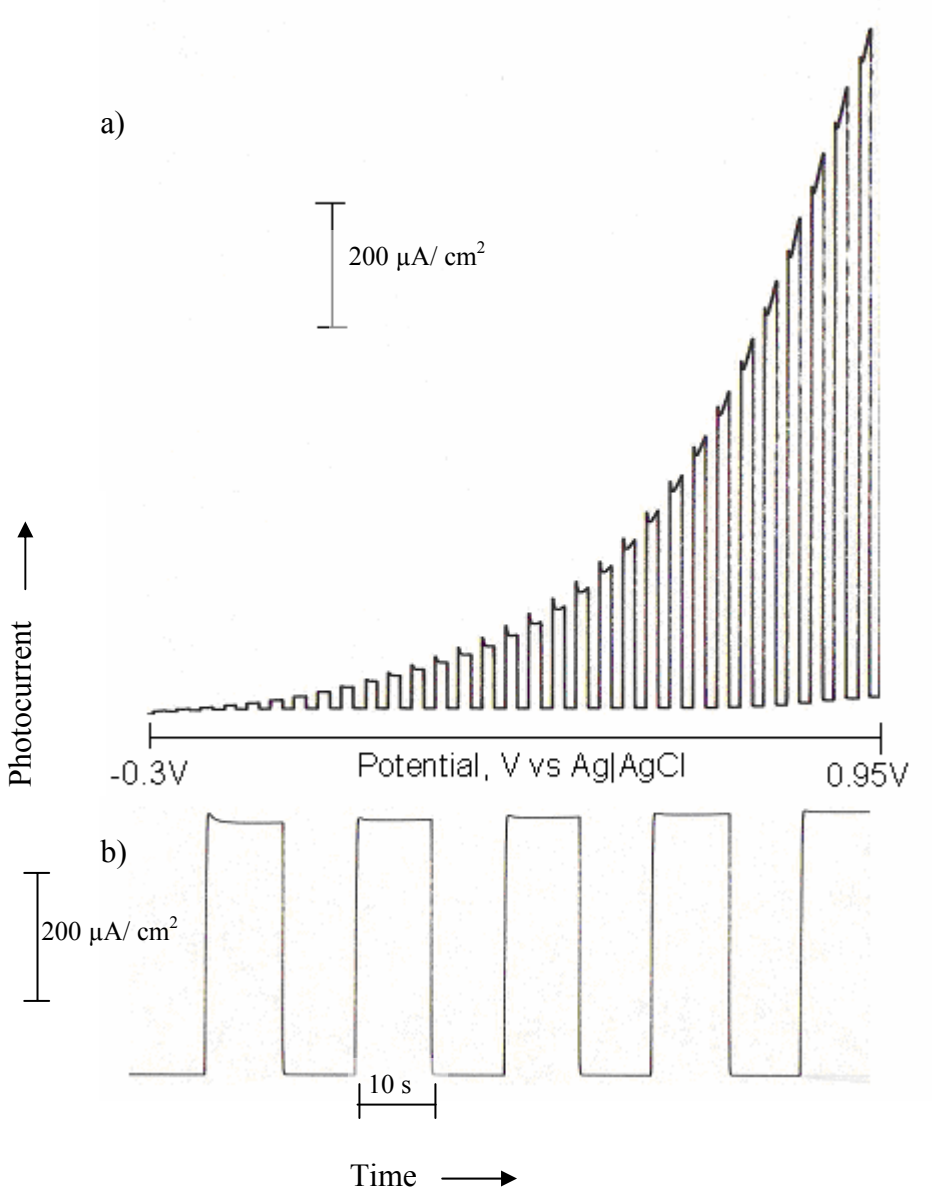

Figure 3.24 A photovoltammogram at 0.1 Hz chopped irradiation (a) and transient photocurrent profile (b) for a $(CdO)_x(ZnO)_{1-x}$ film electrodeposited from a bath at 90:10 (Zn^{2+}:Cd^{2+} ratio) 0.1 M Na_2SO_4. The film was electrodeposited on a TCO substrate. Photovoltammograms were obtained at 2 mV/s; the full output of 75 W xenon arc lamp was used in both sets of experiments. The transients in Figure 3.24(b) were measured at 0.80 V.

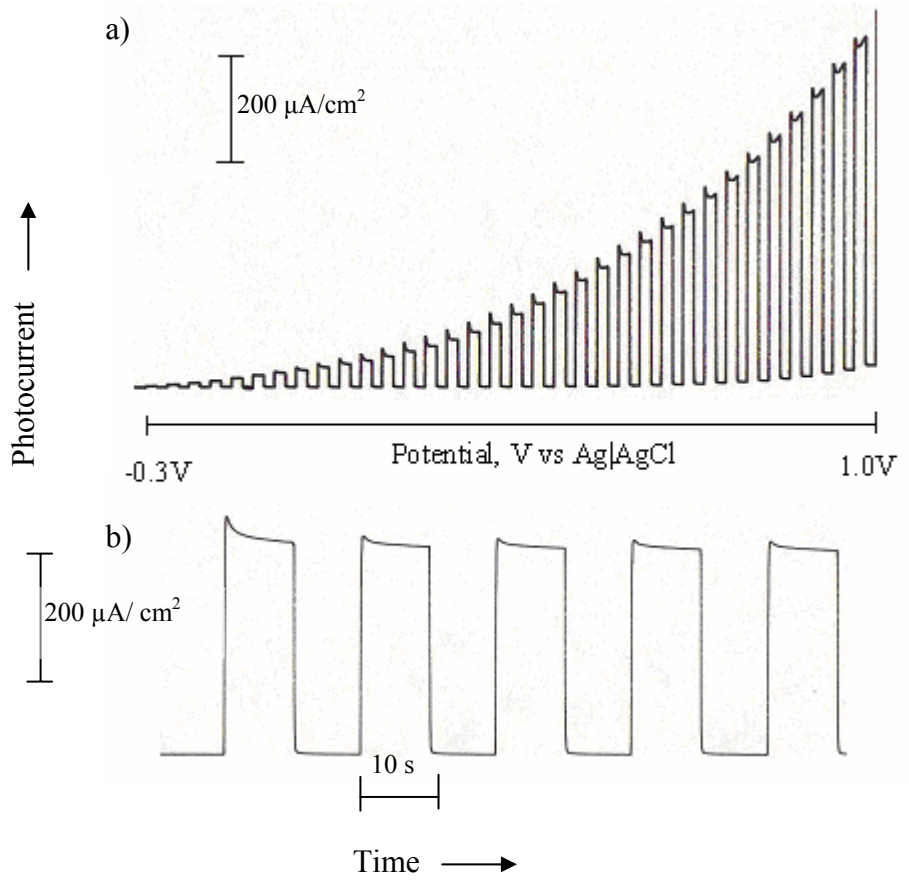

Figure 3.25 A photovoltammogram at 0.1 Hz chopped irradiation (a) and transient photocurrent profile (b) for a $(CdO)_x(ZnO)_{1-x}$ film electrodeposited from a bath at 70:30 (Zn^{2+}:Cd^{2+} ratio) 0.1 M Na_2SO_4. The film was electrodeposited on a TCO substrate. Photovoltammograms were obtained at 2 mV/s; the full output of 75 W xenon arc lamp was used in both sets of experiments. The transients in Figure 3.25(b) were measured at 0.80 V.

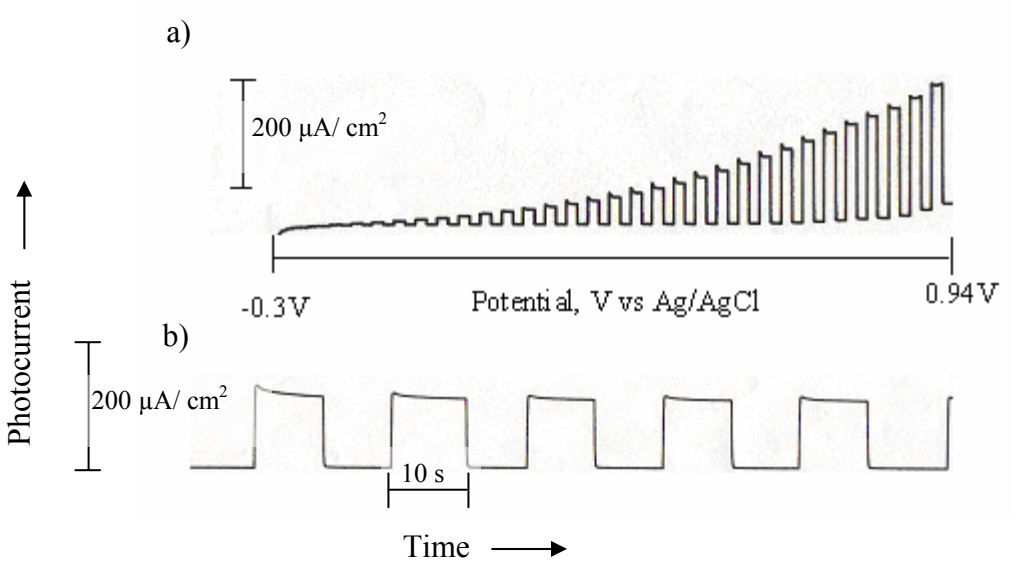

Figure 3.26 A photovoltammogram at 0.1 Hz chopped irradiation (a) and transient photocurrent profile (b) for a $(CdO)_x(ZnO)_{1-x}$ film electrodeposited from a bath at 50:50 (Zn^{2+}:Cd^{2+} ratio) 0.1 M Na_2SO_4. The film was electrodeposited on a TCO substrate. Photovoltammograms were obtained at 2 mV/s; the full output of 75 W xenon arc lamp was used in both sets of experiments. The transients in Figure 3.26(b) were measured at 0.80 V.

CHAPTER 4

CONCLUDING REMARKS

In summary, CdO thin films were successfully electrodeposited on TCO substrates using the cathodic base electrogeneration approach in an aqueous medium containing Cd^{2+} species and dissolved O_2. Further efforts will be directed at a fuller understanding of the sensitivity of the film composition and non-stoichiometry to the deposition variables as well as the mechanistic aspects of the deposition process itself.

$(ZnO)_x(CdO)_{1-x}$, mixed oxide films were successfully electrodeposited on TCO substrates. A variation in band gap is observed in films with different ratios of ZnO and CdO. An improvement in the stability of the photocurrent from ZnO is observed when a small amount of CdO is present in the film matrix. Further efforts must be directed toward tuning the band gap by varying the concentration of Zn^{2+} and Cd^{2+} species in solution. This would allow possible variations in the band-gap of the mixed oxide films between 2.1 eV-3.3 eV. Apart from this, the electrodeposition must be carried out at potentials less negative than -0.8 V, which would be more favorable for pure CdO phase formation. The mechanistic aspects of the deposition process must be elucidated and surface analysis studies are needed.

REFERENCES

1. D. Lincot, *Thin Solid Films* (in press); available online at www.sciencedirect.com.
2. C. Natarajan and G. Nogami, *J. Electrochem. Soc.*, **143**, 1547 (1996).
3. I. Zhitomirsky, *Nanostructured Materials*, **8**, 521 (1997).
4. N. R. de Tacconi, C. R. Chenthamarakshan, K. Rajeshwar, *ECS Proceedings*, **17**, 28 (2003).
5. N. R. de Tacconi, C. R. Chenthamarakshan, K. L. Wouters, F. M. MacDonnell and K. Rajeshwar, *J. Electroanal. Chem.*, **566**, 249 (2004).
6. E. A. Meulenkamp, *J. Electrochem. Soc.*, **144**, 1664 (1997).
7. T. Pauporté, *J. Electrochem. Soc.*, **149**, C539 (2002).
8. A. E. Rakshani, *Solid State Electronics*, **29**, 7 (1986).
9. G. H. A. Therese and P. V. Kamath, *Chem. Mater.*, **12**, 1195 (2000).
10. P. E. de Jongh, D. Vanmaekelbergh and J. J. Kelly, *Chem. Commun.*, 1069 (1999).
11. J. A. Switzer, *Am. Ceram. Bull.*, **66**, 1521 (1987).
12. N. R. de Tacconi, C. R. Chenthamarakshan, K. Rajeshwar, T. Pauporté and D. Lincot, *Electrochem. Commun.*, **5**, 220 (2003).
13. K. Rajeshwar, N. R. de Tacconi and C. R. Chenthamarakshan, *Curr. Opinion Solid State Mater. Sci.*, **8**, 173 (2004).
14. F. P. Koffyberg, *J. Solid State Chem.*, **2**, 176 (1970).
15. F. P. Koffyberg, *Can. J. Phys.*, **49**, 435 (1971).

16. F. P. Koffyberg, *Solid State Commun.*, **9**, 2187 (1971).

17. F. A. Benko and F. P. Koffyberg, *Solid State Commun.*, **57**, 901 (1986).

18. K. Maschke and U. Rossler, *Phys. Stat. Sol.*, **28**, 577 (1968).

19. A. Breeze and P.G. Perkins, *Solid State Commun.*, **13**, 1031 (1973).

20. K. Kawamura, K. Maekaun, H. Yanagi, M. Hirano and H. Ozono, *Thin Solid Films*, **445**, 182 (2003).

21. T. L Chu and S. S. Chu, *J. Electron. Mater.*, **19**, 1002 (1990).

22. Y. Homes and S. E. San, *Solar Energy*, **77**, 291 (2004).

23. H. H. Kung, H. S. Jarrett, A. W. Sleight and A. Ferretti, *J. Appl. Phys.*, **48**, 2463 (1977).

24. M. A. Butler and D. S. Girley, *J. Electrochem. Soc.*, **125**, 228 (1978).

25. D. Makuta, S. K. Poznyak and A. I. Kulak, *Solid State Commun.*, **76**, 65 (1990).

26. L. M. Su, N. Grote and F. Schmitt, *Electron. Lett.*, **20**, 716 (1984).

27. M. Ortega, G. Santana and A. Morales-Acevedo, *Solid State Electron.*, **44**, 1765 (2000).

28. A. Shiori, *Japanese Patent*, **7**, 909 (1979).

29. V. M. Aroutiounian, V. M. Arakelyan and G. E. Shahnazaryan, *Solar Energy*, **78**, 581 (2005).

30. K. Gurumurugan, D. Mangalraj, S. K. Narayandass, Y. Nakanishi and Y. Hatanaka, *Appl. Surf. Sci.*, **113/114**, 422 (1997).

31. T. K. Subramanyam, B. S. Naidu and S. Uthanna, *Appl. Surf. Sci.*, **169/170**, 529 (2001).

32. D. Ma, Z. Ye, L. Wang, J. Huang and B. Zhao, *Mater. Lett.*, **58**, 128 (2003).

33. T. R. Reddy, C. Sraveni and R. W. Miles, *J. Cryst. Growth*, **184/185**, 1031 (1998).

34. F. C. Eze, *Mater.Chem. Phys.*, **89**, 205 (2005).

35. K. Gurumurugan, D. Mangalraj and S. K. Narayandass, *J. Cryst. Growth*, **147**, 355 (1995).

36. N. Benramdane, W. A. Murad, R. H. Misho, M. Ziane and Z. Kebbab, *Mater. Chem. Phys.*, **48**, 119 (1997).

37. R. Ferro and J. A. Rodríguez, *Thin Solid Films*, **347**, 295 (1999).

38. M. D. Uplane, P. N. Kshirsagar, B. J. Lokhande and C. H. Bhosale, *Mater. Chem. Phys.*, **64**, 75 (2000).

39. R. Ferro and J. A. Rodríguez, *Solar Energy Mater. Solar Cells*, **64**, 363 (2000).

40. B. J. Lokhande, P. S. Patil and M. D. Uplane, *Mater. Chem. Phys.*, **84**, 238 (2004).

41. C. H. Bhosale, A. V. Kambale, A. V. Kokate and K. Y. Rajpure, *Mater. Science Eng. B*, **122**, 67 (2005).

42. Y.-S. Choi, C.-G. Lee and S. M. Cho, *Thin Solid Films*, **289**, 153 (1996).

43. D. M. Carballeda-Galicia, R. Castanedo-Pérez, O. Jiménez-Sandoval, S. Jiménez-Sandoval, G. Torres-Delgado and C. I. Zúñiga-Romero, *Thin Solid Films*, **371**, 105 (2000).

44. P. K. Ghosh, R. Maity and K. K. Chattopadhyay, *Solar Energy Mater. Solar Cells*, **81**, 279 (2004).

45. R. Maity and K. K. Chattopadhyay, *Solar Energy Mater. Solar Cells* (in press); available online at www.sciencedirect.com.

46. H. Hobert and B. Seltmann, *J. of Non-Crystalline Solids*, **195**, 54 (1996).

47. N. Matsuura, D.J. Johnson and D.T. Amm, *Thin Solid Films*, **295**, 260 (1997).

48. Z. Zhao, D. L. Morel and C. S. Ferekides, *Thin Solid Films*, **413**, 203 (2002).

49. A. Gulino and G. Tabbi, *Appl. Surf. Sci.*, **245**, 322 (2005). See also references therein.

50. I. J. Ferrer, *Electrochim. Acta*, **38**, 2199 (1993).

51. R. Jayakrishnan and G. Hodes, *Thin Solid Films*, **440**, 19 (2003).

52. D. Gruber, F. Kraus and J. Muller, *Sensors and Actuators B*, **92**, 81 (2003).

53. S. T. Shishiyanu, T. S. Shishiyanu and O. I. Lupan, *Sensors and Actuators B*, **107**, 379 (2005).

54. G. Ferblantier, F. Mailley, R. Al Asmar, A. Foucaran and F. Pascal-Delannoy, *Sensors and Actuators A* (in press); available online at www.sciencedirect.com.

55. S. S. Lee and R. M. White, *Sensors and Actuators A*, **52,** 41 (1996).

56. L. Znaidi, G. J. A. A. Soler Illia, S. Beyahia, C. Sanchez andA.V. Kanaev, *Thin Solid Films*, **428**, 257 (2003).

57. W.W. Wang, X.G. Diao, Z. Wang, M. Yang, T.M. Wang and Z. Wu, *Thin Solid Films* (in press); available online at www.sciencedirect.com.

58. H. Ko, W. P Tai, K. C Kim, S. H. Kim, S. J Suh and Y.S Kim, *J. Crystal Growth*, **277**, 352 (2005).

59. B.G. Choi, I.H. Kim, D.H Kim, K.S. Lee, T.S. Lee, B. Cheong, Y.-J. Baik and W.M. Kim, *J Eur. Ceram. Soc.,* **25**, 2161 (2005).

60. A. D. Compaan, A. Gupta, S. Lee, S. Wang and J. Drayton, *Solar Energy*, **77**, 815 (2004).

61. Y. M. Lu, C. M Chang , S. I. Tsai and T. S Wey, *Thin Solid Films,* **447-448**, 56 (2004).

62. C. Agashe, O. Kluth, G. Schöpe, H. Siekmann, J. Hüpkes and B. Rech, *Thin Solid Films,* 442, **167** (2003).

63. D. Herrmann, M. Oertel, R. Menner and M. Powalla, *Surface and Coatings Technology,* **174-175**, 229 (2003)

64. J. M. Ting and B. S. Tsai, *Mater. Chem. Phys.*, **72**, 273 (2001).

65. S. Bandyopadhyay, G. K. Paul and S. K. Sen, *Solar Energy Mater. Solar Cells*, **71**, 103 (2002).

66. Y. Natsume and H. Sakata, *Thin Solid Films*, **372**, 30 (2000).

67. D. Bao, H. Gu and A. Kuang, *Thin Solid Films*, **312**, 37 (1998).

68. M.H. Aslan, A.Y. Oral, E. Mensur, A. Gul and E. Basaran, *Solar Energy Mater. Solar Cells*, **82**, 543 (2004).

69. S. Faÿ, U. Kroll, C. Bucher and E. V. Sauvain and A. Shah, *Solar Energy Mater. Solar Cells,* **86**, 385 (2005).

70. T. M. Barnes, J. Leaf, C. Fry and C. A. Wolden, *J. Cryst. Growth*, **274**, 412 (2005).

71. J. Nishino and Y. Nosaka, *J. Cryst. Growth,* **268**, 174 (2004).

72. H. Deng, J. J. Russell, R. N. Lamb, B. Jiang, Y. Li and X. Y. Zhou, *Thin Solid Films,* **458**, 43 (2004).

73. Y. Kashiwaba, K. Sugawara, K. Haga, H. Watanabe, B. P. Zhang and Y. Segawa, *Thin Solid Films*, **411**, 87 (2002).

74. M. Quintana, E. Ricra, J. Rodríguez and W. Estrada, *Catalysis Today,* **76**, 141 (2002).

75. J. L. Zhao, X. Li, J. M. Bian, W.D. Yu and C.Y. Zhang, *J. Cryst. Growth*, **280**, 495 (2005).

76. A. Bougrine, M. Addou, A. Kachouane, J. C. Bérnède and M. Morsli, *Mater. Chem. Phys.,* **91**, 247 (2005).

77. H. Gomez, A. Maldonado, M. L. Olvera and D.R. Acosta, *Solar Energy Mater. Solar Cells*, **87**, 107 (2005).

78. Di Li and H. Haneda*, J. Photochem. Photobiol. A: Chem.,* **160**, 203 (2003).

79. P. Fons, K. Iwata, S. Niki, A. Yamada and K. Matsubara, *J. Cryst. Growth*, **201-202***,* 627 (1999)

80. K. Ramamoorthy, C. Sanjeeviraja, M. Jayachandran, K. Sankaranarayanan, P. Bhattacharya and L. M. Kukreja, *J. Cryst. Growth,* **226**, 281 (2000).

81. R. Triboulet and J. Perrière, *Progress in Cryst. Growth and Characterization of Mater.,* **47**, 65 (2003).

82. S. Peulon and D. Lincot, *Adv. Mater*., **8,** 166 (1996).

83. M. Izaki and T. Omi, *Appl. Phys. Lett*., **68,** 2439 (1996).

84. T. Pauporté and D. Lincot, *Appl. Phys. Lett.*, **75**, 3817 (1999).

85. A. Goux, T. Pauporté, J. Chivot and D. Lincot*, Electrochim. Acta*, **50,** 2239 (2005).

86. T. Pauporté and D. Lincot, *Electrochim. Acta*, **45,** 3345 (2000).

87. T. Pauporté and D. Lincot, *J. Electroanal. Chem.*, **517**, 54 (2001).

88. T. Mahalingam, V. S. John, M. Raja, Y. K. Su and P. J. Sebastian, *Solar Energy Mater. Solar Cells*, **88**, 227 (2005).

89. S. Karuppuchamy, K. Nonomura, T. Yoshida, T. Sugiera and H. Minoura, *Solid State Ionics*, **151**, 19 (2002).

90. L. Zhang, Z. Chen, Y. Tang, Y. Tang and Z. Jia, *Thin Solid Films* (in press); available online at www.sciencedirect.com.

91. T. Yoshida, D. Komatsu, N. Shimokawa and H. Minoura, *Thin Solid Films,* **451** (2004).

92. T. Pauporté and D. Lincot, *J. Electrochem. Soc.*, **148**, 310 (2001).

93. Joint Committee for Powder Diffraction Studies (JCPDS) File No. 05-0640.

94. B. D. Cullity, *Elements of X-Ray Diffraction*, Addison-Wesley, Reading, MA (1967).

95. Joint Committee for Powder Diffraction Studies (JCPDS) File No. 36-1451.

BIOGRAPHICAL INFORMATION

The author received his Master of Science in Materials Science and Engineering from The University of Texas at Arlington in August 2005. He received his Bachelor of Engineering in Manufacturing Science and Engineering from Visveswaraiah Technological University in June 2003.